

Pion double charge exchange and inelastic scattering on ^3He

M. Yuly,* W. Fong,† E. R. Kinney,‡ C. J. Maher,§ J. L. Matthews, T. Soos,|| J. Vail,¶ M. Y. Wang,** and S. A. Wood††
*Department of Physics and Laboratory for Nuclear Science, Massachusetts Institute of Technology,
 Cambridge, Massachusetts 02139*

P. A. M. Gram‡‡
Los Alamos National Laboratory, Los Alamos, New Mexico 87545

G. A. Rebka, Jr. and D. A. Roberts§§
Department of Physics, University of Wyoming, Laramie, Wyoming 82071
 (Received 7 June 1995; revised manuscript received 9 December 1996)

Measurements were made of the doubly differential cross sections for three inclusive pion reactions on ^3He : π^- double charge exchange (DCX), and π^+ and π^- inelastic scattering. The cross sections for DCX were measured at incident pion energies of 120, 180, and 240 MeV, and at angles of 25° , 50° , 80° , 105° , and 130° , while inelastic scattering cross sections were measured at 120, 180, and 240 MeV and scattering angles of 50° , 80° , 105° , and 130° . In each case the outgoing pion energy spectra were measured from 10 MeV up to the kinematic limit. The DCX spectra exhibit a double-peaked structure at forward angles that can be understood as a consequence of a sequential single charge exchange mechanism. Model calculations based on this mechanism are in rough agreement with the measured spectra. The doubly differential cross sections measured for the inelastic scattering reactions exhibit a prominent quasielastic peak. A distorted-wave impulse-approximation calculation of the quasielastic cross sections has been performed and a comparison made with the measurements. [S0556-2813(97)01204-1]

PACS number(s): 25.80.Ek, 25.80.Gn, 25.80.Ls, 27.10.+h

I. INTRODUCTION

Much recent research has focused on the interactions of pions with individual nucleons. A complete description of the πN interaction, however, although useful in understanding many of the interactions between pions and nuclei, is insufficient to explain all possible nuclear reactions. Processes such as absorption, intermediate Δ propagation within the nucleus, and multiple scattering all require the presence of more than one nucleon. One motivation for the research described in this work is to gain a better understanding of the role of double scattering in pion-nucleus reactions by comparing reactions in a single nucleus to which double scattering contributes different amounts. The reactions observed

were inclusive double charge exchange (DCX), $^3\text{He}(\pi^-, \pi^+)3n$, and inclusive inelastic scattering, $^3\text{He}(\pi^-, \pi^-)$ and $^3\text{He}(\pi^+, \pi^+)$.

The fact that, at Δ -resonance energies, positive pions scatter preferentially from protons while negative pions scatter preferentially from neutrons can be exploited to gain a qualitative understanding of the amount of double scattering to expect in each of these processes. The reaction $^3\text{He}(\pi^-, \pi^-)$ proceeds primarily through single scattering from the sole neutron in ^3He . The DCX reaction, $^3\text{He}(\pi^-, \pi^+)$, requires that at least both protons be involved to conserve charge. The simplest mechanism which can describe this reaction, the sequential single charge exchange (SSCX) mechanism shown schematically in Fig. 1(a), is inherently a double scattering process. For $^3\text{He}(\pi^+, \pi^+)$, in which the scattering takes place primarily from one or both of the two protons, one expects both single and double scattering to occur. One therefore expects a much larger contribution from double scattering processes in $^3\text{He}(\pi^+, \pi^+)$ than in $^3\text{He}(\pi^-, \pi^-)$, and the double scattering component of the inelastic cross section should be closely related to the magnitude of the DCX cross section.

II. PREVIOUS EXPERIMENTAL WORK

A. Double charge exchange (DCX)

The earliest inclusive DCX measurements were made at the JINR Synchro-cyclotron in Dubna by Batusov *et al.* [1] using nuclear emulsions. Later experiments by Batusov *et al.* [2] and Gilly *et al.* [3] were performed in which total DCX cross sections on a range of nuclei from He to Pb were measured. After this pioneering work, most inclusive DCX ex-

*Present address: Department of Physics, Northwest Nazarene College, Nampa, ID 83686.

†Present address: ROCS, Carlsbad, CA 92009.

‡Present address: Department of Physics, University of Colorado, Boulder, CO 80309.

§Present address: Pittsburgh Supercomputing Center, Pittsburgh, PA 15213.

||Present address: 93 Jackson St., Cambridge, MA 02140.

¶Present address: 7 Brattle Street #4, Arlington, MA 02174.

**Present address: The Rand Corporation, Santa Monica, CA 90406.

††Present address: Thomas Jefferson National Accelerator Facility, Newport News, VA 23606.

‡‡Present address: P.O. Box 173, Captain Cook, HI 96704.

§§Present address: Department of Physics, University of Michigan, Ann Arbor, MI 48109.

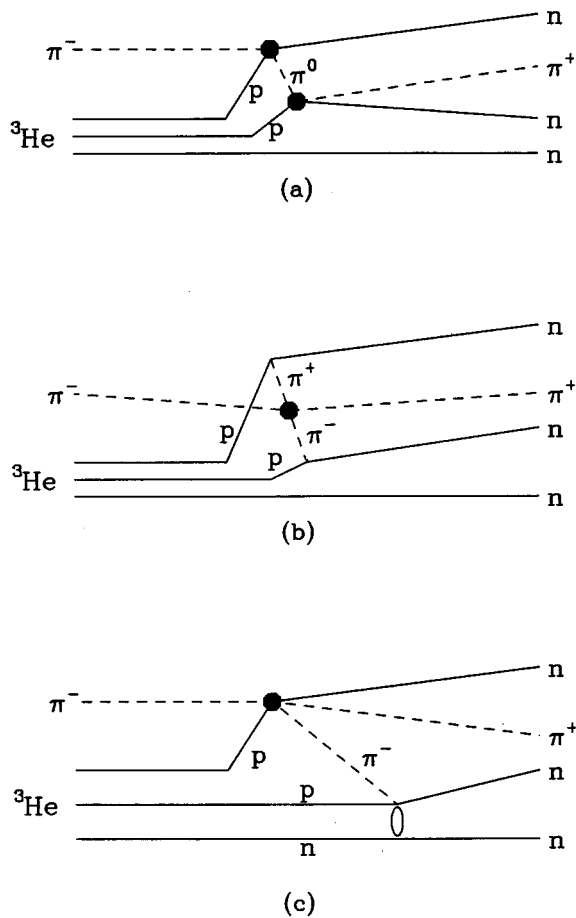


FIG. 1. Schematic diagram of (a) the SSCX mechanism, (b) the meson-exchange mechanism of Germond and Wilkin [43], and (c) the pn absorption mechanism of Jeanneret *et al.* [6] for the ${}^3\text{He}(\pi^-, \pi^+)3n$ reaction.

periments concentrated primarily on the ${}^4\text{He}$ nucleus, using bubble [4–6] and spark [7] chambers, often in a search for tetra-neutron states. The first modern measurement [8] of doubly differential cross sections for inclusive DCX was made at the Schweizerisches Institut für Nuklearforschung (SIN, now the Paul Scherrer Institute, or PSI) for the ${}^{16}\text{O}(\pi^+, \pi^-)$ reaction.

Two previous experiments have examined the DCX reaction in ${}^3\text{He}$. The first, published by Sperinde *et al.* [9] in 1970, used the Berkeley 4.6 m cyclotron in a search for a three-neutron resonance. Only one spectrum was measured, for 140 MeV incident pions at an average scattering angle of about 30° , with detected outgoing pions having kinetic energies between 40 and 125 MeV. The measured spectrum differed significantly from pure four-body phase space,¹ exhibiting instead a double-peaked structure. This was originally interpreted as a possible tri-neutron resonance. It was later shown by Phillips [10], however, that interactions between two of the nucleons in the final state could account for the

¹Phase space is the cross section distribution obtained if one assumes that the matrix element, which contains the “physics” of the problem, is constant. Thus, four-body phase space corresponds to $\pi + A \rightarrow \pi + N + N + (A - 2)$.

shape of the DCX spectrum. The second experiment was performed by Stetz *et al.* [11] at the Clinton P. Anderson Meson Physics Facility (LAMPF) using the EPICS spectrometer. These results consist of doubly differential cross sections at 140 MeV for laboratory angles of 20° , 30° , 50° , and 80° , at 200 MeV for 23.5° , and at 295 MeV for 30° and 120° . The double-peaked structure is also seen in these measurements, although the resonance parameters computed for the high-energy peak depend on the incident energy and scattering angle, thereby virtually eliminating the possibility of a tri-neutron resonance. These measurements had relatively large uncertainties. Moreover, the measurements of Stetz *et al.* and Sperinde *et al.* made at the same incident energy and scattering angle disagree at high outgoing pion energies.

An extensive study of the ${}^4\text{He}(\pi^+, \pi^-)$ and ${}^4\text{He}(\pi^-, \pi^+)$ reactions, over the incident energy range 120–240 MeV, with good statistical accuracy and complete coverage of the outgoing pion energy spectrum, revealed a double-peaked structure at forward angles in this nucleus as well [12,13]. This result is in striking contrast to the spectra seen in DCX on heavier nuclei (${}^{16}\text{O}$ to ${}^{208}\text{Pb}$) [14], in which this structure is absent, and which roughly resemble the distribution of events in four-body phase space.

B. Inelastic scattering

As with the DCX measurements, the earliest measurements of inelastic pion scattering were made with nuclear emulsions [15]. Later measurements were made on a variety of target nuclei using cloud chambers [16–18] and scintillation counters [19,20] to detect the outgoing particles. The first modern experiment to measure inelastic pion-nucleus scattering was performed by Binon *et al.* [21] at the CERN Synchro-cyclotron.

Inclusive inelastic scattering of pions from the ${}^3\text{He}$ nucleus has been studied near the Δ resonance in three previous experiments. The earliest results were published by Whitney *et al.* [22]. In this experiment, the doubly differential cross sections for the ${}^3\text{He}(\pi^+, \pi^+)$ and ${}^3\text{He}(\pi^-, \pi^-)$ reactions were measured using the EPICS spectrometer at LAMPF at 60° and 120° for 200 MeV incident pions, and at 120° for 295 MeV incident pions. A later experiment, performed by Klein *et al.* [23] at SIN (now PSI), used the SUSI spectrometer to detect the outgoing pions. This experiment measured outgoing pion energy spectra at 170, 220, 270, and 320 MeV incident pion energy over a broad range (45° – 135°) of angles. Recently, a third experiment has been reported by Khandaker *et al.* [24,25] which measured inclusive inelastic scattering on ${}^2\text{H}$, ${}^3\text{He}$, and ${}^4\text{He}$ at 96.5 MeV and at angles from 40° to 125° . This measurement was made at the Tri-University Meson Facility (TRIUMF) using the QQD spectrometer. In all of the previous experiments, the measured spectra exhibit a prominent peak located very near the outgoing energy for scattering from a free nucleon. One can conclude therefore that the inelastic scattering process in ${}^3\text{He}$ is dominated by quasifree interactions with single nucleons.

III. EXPERIMENTAL APPARATUS AND PROCEDURE

The present experiment was performed at LAMPF using a 180° vertical bend, double-focusing magnetic spectrometer.

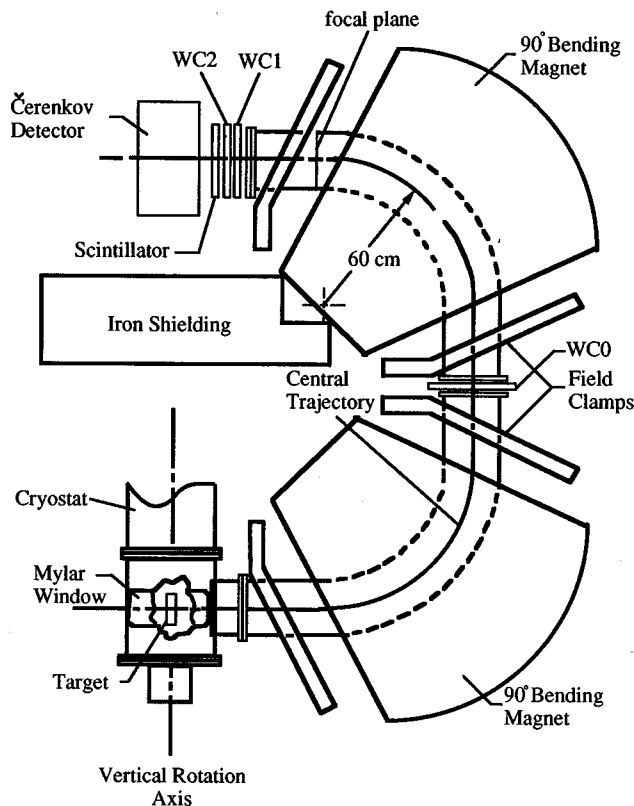


FIG. 2. Drawing of the 180° vertical bend, double-focusing magnetic spectrometer. Pions travel through vacuum from the target, through two 90° dipole magnets, to the focal plane. There is a 2.5 cm break in the vacuum for WC0, the midspectrometer wire chamber, which is used to require that a particle traverses the entire spectrometer. Particle trajectories are traced back to the focal plane using information from two wire chambers, WC1 and WC2. The scintillator is used to distinguish positive pions from protons, as well as to provide TOF information. The Čerenkov detector separates pions from electrons and positrons.

The experimental apparatus and procedure are very similar to those of Wood *et al.* [14,26].

The 120–240 MeV incident π^\pm beam from the high-energy pion channel (“P³”) first passed through an ionization chamber, which was used to determine the relative flux. Since this device was sensitive to all charged particles in the beam, it was necessary to normalize the flux measurement each time the beam transport elements were adjusted. The size (about 1.6 cm in diameter) and position of the beam spot were continuously monitored by a small multiwire proportional chamber placed downstream of the ionization chamber and 30 cm upstream of the target. Downstream of the target, the pion beam struck a 6 mm thick polyethylene (CH₂) target. Three-element plastic scintillator telescopes were placed on each side of the CH₂ target to detect pions scattered at 90° . These telescopes were used to monitor the position of the incident beam, as well as to provide a check on the flux determined by the ionization chamber. The response of the telescopes was sensitive essentially only to pions, since beam contaminants are very unlikely to scatter at 90° into the telescopes.

The spectrometer (shown in Fig. 2) has an effective solid angle of about 16 msr and a momentum bite of about 8%. It

focuses in both the horizontal and vertical directions so the detector system could be relatively small, and it requires no detectors at the entrance to the spectrometer, allowing higher luminosities to be used. The 180° vertical bend of the magnet provides stringent selection of the charge of the detected particle. Finally, the short flight path (3.5 m), which was entirely in vacuum except for a 2.5 cm interruption for a midspectrometer wire chamber, allowed low-energy pions to reach the focal plane with minimal corrections for scattering and decay.

The detector system had five components: a wire chamber (WC0) placed in the mid-plane of the spectrometer, two wire chambers (WC1 and WC2) near the focal plane that were used to reconstruct trajectories, behind these, a 1.6 mm scintillator (S1), that provided an accurate time reference for the trigger as well as pulse height information useful in the identification of particles, and lastly a fluorocarbon (FC-88) Čerenkov detector that distinguished electrons from pions. The anode and one of the cathode planes of each wire chamber [27] consisted of orthogonal arrays of wires. Position information in two dimensions was obtained from a delay-line readout of individual wire signals.

The trigger was a fourfold coincidence among the three wire chambers and the scintillator. The information recorded in each event comprised the pulse heights of the signals from the scintillator and the Čerenkov detectors and the delay times of the signals from the wire chambers. Inclusion of the midspectrometer wire chamber guaranteed that a particle had passed through the spectrometer, which accomplished a crucial reduction of the trigger rate due to room background. The timing information available from this chamber was also used to distinguish pions from very slow protons.

Liquid ^3He was condensed from a closed volume into the target flask by passage through condensing coils immersed in a ^4He bath maintained at a temperature below the λ point by pumping. The ^4He reservoir could be replenished continuously from a 500 l storage Dewar through a “helitran” transfer tube, allowing uninterrupted operation of the target cryostat for several days at a time. The target flask was a vertical cylinder 25 mm in diameter and 75 mm high with a $51\ \mu\text{m}$ thick Mylar wall. It was surrounded by 4 layers of $0.64\ \mu\text{m}$ aluminized Mylar superinsulation and, at a radius of 19 cm, a $13\ \mu\text{m}$ aluminum heat shield maintained at liquid nitrogen temperature. The insulating vacuum of the cryostat was contiguous with that of the spectrometer vacuum chamber.

The pressures of the saturated vapor in equilibrium with the liquid in both the bath and the target flask were measured by redundant precision gauges. These measurements were recorded continuously throughout the experiment to establish the density of the ^3He liquid in the target.

The target flask, an identical empty flask, and a CH (styrofoam) cylinder of the same dimensions as the flasks were arrayed vertically on the axis of rotation of the spectrometer. An elevator mechanism could position each of the three targets in the path of the beam, permitting convenient measurement of the empty target background and of πp scattering, which was the reference cross section in this experiment.

To measure the doubly differential cross sections the target was exposed to an incident pion beam and events were collected at given spectrometer momentum settings until sta-

tistical uncertainties of approximately 5% in the number of detected pions were achieved. Data were collected at 10 MeV intervals in outgoing pion energy. In addition to each complete set of ^3He observations, a series of observations was made measuring the background from the empty target walls. This process was repeated for each spectrometer angle and incident energy. Each time the incident energy, and hence the normalization of the beam monitors, was changed, a series of CH normalizations at different spectrometer angles was performed.

Doubly differential cross sections for the $^3\text{He}(\pi^-, \pi^+)$ reaction were measured for outgoing pion kinetic energies from 10 MeV up to the kinematic limit at incident energies of 120, 180, and 240 MeV for scattering angles of 25° , 50° , 80° , 105° , and 130° , and 25° and 50° at an incident energy of 210 MeV. The $^3\text{He}(\pi^+, \pi^+)$ and $^3\text{He}(\pi^-, \pi^-)$ cross sections were measured over the same outgoing pion energy range, at incident energies of 120, 180, and 240 MeV for scattering angles of 50° , 80° , 105° , and 130° . Observation of the inelastic scattering reactions at 25° was prevented by a large background due to the spectrometer intercepting the beam.

IV. DATA ANALYSIS

The goal of this experiment was to measure a doubly differential cross section for each reaction, incident pion energy, scattering angle, and outgoing pion energy studied. The doubly differential cross section is related to observable quantities as follows:

$$\frac{d^2\sigma}{d\Omega dE_\pi} = \frac{N_{\text{det}}\epsilon_c}{N_{\text{inc}}\Delta\Omega\Delta E_\pi x\rho f_d f_l}, \quad (1)$$

where N_{det} is the number of pions detected, N_{inc} is the number of pions that were incident, x is the effective thickness of the target, ρ is the density of the target, $\Delta\Omega$ is the effective solid angular acceptance, ΔE_π is the range of outgoing pion energy, ϵ_c is a correction of the spectrometer acceptance due to multiple scattering and energy loss, f_d is the correction due to pion decay, and f_l is the dead-time correction.

The analysis proceeded in eight steps.

A. Wire chamber calibration and phase space definition

Calibration constants relating time differences of signals from wire chambers to position were established by placing a collimated ^{55}Fe source at precisely measured positions in front of the chambers. For each event, the position information from WC1 and WC2 was used to reconstruct the particle trajectory back to the focal plane of the spectrometer. Reconstructed trajectories were tested for conformity with the distribution in phase space of particles that could have been transmitted from the target to the focal plane by the spectrometer.

B. Particle identification

To calculate cross sections it was necessary to separate the pions from the other particle species that also caused triggers. Protons were generally eliminated by their large pulse heights in the scintillator. At a spectrometer setting of

about 156 MeV/c, where the protons were just reaching the scintillator, however, many of the protons deposited the same amount of energy as the pions in the scintillator. In this case, the protons were distinguished by their longer time-of-flight (TOF) between WC0 and S1.

Since pions, as well as electrons,² emit Čerenkov radiation at spectrometer settings greater than 180 MeV/c ($T_\pi = 88$ MeV), it was not possible to use the Čerenkov detector to distinguish electrons from pions on an event-by-event basis. Instead, a more indirect method was used. In general, the number of pions can be written:

$$N_\pi = \frac{N^< - f_e^< N_{\text{total}}}{f_\pi^< - f_e^<}, \quad (2)$$

where N_π is the number of pions to be determined, $N^<$ is the total number of particles that emit less than a certain amount of Čerenkov light, N_{total} is the total number of events, and $f_e^<$ and $f_\pi^<$ are the fractions of electrons and pions, respectively, which emit less than the chosen amount of Čerenkov light given a pure electron or pion source. A similar equation exists using the number of particles that emit more than the selected amount of Čerenkov light, $N^>$. The dependence of the random uncertainty in N_π on the Čerenkov light cutoff was shown to be relatively flat over a large range of channels [28], and the cutoff corresponding to the minimum uncertainty was selected. The fraction of electrons, $f_e^<$, was determined at a spectrometer setting of 53.8 MeV/c, where it was possible to separate the electrons from the pions using the pulse heights in S1. This fraction was used for all spectrometer settings, since at these momenta $\beta \approx 1$ for electrons, and the Čerenkov spectrum depends only on β . The pion fraction, $f_\pi^<$, was determined for each spectrometer setting by observing inelastic scattering and assuming the spectrum to be purely pions with no electron contamination. This assumption is reasonable, since the cross sections for reactions which produce electrons are much smaller than the quasielastic scattering cross section.

C. Acceptance and dispersion

The momentum acceptance, $\Delta p/p$, and dispersion were determined by scanning a peak (either a ^3He quasielastic peak or a πp elastic scattering peak from the CH target) across the spectrometer focal plane by changing the spectrometer magnetic field. The changing acceptance across the focal plane resulted in changes in the observed area of the peak. The relative acceptance as a function of focal plane position was determined by this method, and was used to correct N_π . The effective total momentum acceptance was determined to be about 8% by integration across the entire focal plane. Measurement of the acceptance at a single central momentum suffices to establish the performance of the spectrometer when associated with the extensive measurements of the magnetic field configuration that have previously been made for these magnets. These show the configura-

²Electrons or positrons, depending on the charge setting of the spectrometer. The word ‘‘electron’’ will be used generically throughout this discussion.

ration to be unchanging over a range of fields extending to over 18 kG. A typical acceptance function is shown in Ref. [14], which also cites references to previous studies of the properties of the spectrometer.

D. Normalization

The absolute number of incident pions, N_{inc} in Eq. (1), was obtained by comparison of πp elastic scattering measurements (from the CH target) with known cross sections determined by interpolation using the energy-dependent phase shift program SCATPI [29]. The effective total solid angle, $\Delta\Omega$, and the effective target thickness, x , were included in this calibration. This procedure was repeated at several scattering angles for each setting of the beam transport system in order to improve the accuracy of the normalization, as well as to check for the presence of angle-dependent effects.

E. Background subtraction

The pions counted with the empty target were primarily those scattered from the walls of the target cell. For DCX the background was typically only about 8%, and never more than 15%, of the full-target rate, and was measured to about 30% accuracy. For inelastic scattering the background was typically 15–30% of the rate with the full target, and was measured with an uncertainty of less than 10%. The measurements with the empty target were treated in the same manner as those with the full target, and properly normalized background data were subtracted point by point from the full-target data.

F. Corrections

Corrections were made to account for other effects that would change the shape and magnitude of the cross section distributions. The number of pions detected was reduced by decay as they traveled from the target to the detectors. Approximately 80% of the pions survived at 200 MeV, while at 10 MeV only 30% survived. Some of the decay muons traversed the spectrometer, while others did not. In fact, it is possible for pions that would not have traversed the spectrometer to decay into muons that could. Since the detector system could not separate the muons from pions, these effects were accounted for by Monte Carlo methods which produced the factor f_d in Eq. (1). This procedure is described in greater detail in Ref. [14]. Muon contamination from pion decay in the spectrometer was simulated with the DECAY TURTLE [30] code. The fraction of muon contamination ranges from 1% at 10 MeV to 20% at 200 MeV outgoing pion kinetic energy. A different Monte Carlo program, MUCLLOUD [12,26], was used to simulate decays in the scattering chamber. MUCLLOUD used the uncorrected cross sections in an iterative procedure to obtain the corrections, which were typically 0–30%. Energy loss and multiple scattering in the target and in WC0 changed the effective acceptance of the spectrometer; these were corrected for by the factor ϵ_c , which was determined by simulation to be different from unity only for outgoing pion energies less than 30 MeV. The maximum value of ϵ_c was about 1.3.

An effect that is commonly observed to distort inelastic scattering spectra, particularly in the large energy-loss region, is so-called “slit scattering,” in which an elastically scattered particle penetrates or scatters from an aperture and appears in the low-energy region of the spectrum. Since the spectrometer used in this experiment had no entrance slit, we did not expect this to be a problem. As a check, the pion yields from a CH₂ target and from a pure ¹²C target of equal thickness were measured. The ratio of the yields of pions elastically scattered from ¹²C was unity, verifying the target thickness equality. For outgoing pion energies below 70 MeV, a ratio of $Y(\text{CH}_2)/Y(^{12}\text{C}) = 1.05 \pm 0.01$ was found,³ independent of energy. This result implies that around 5% of the inelastic yield in this energy region is due to the presence of the πp elastic scattering peak (at 90 MeV, in this case). Since this correction is small and it is not obvious how to apply it to the ³He(π^\pm, π^\pm) spectra, it was ignored. Such a correction would have a negligible effect on the magnitude of the differential and total cross sections and on the uncertainties in these quantities.

G. Integrated cross sections

Integration of the doubly differential cross sections over outgoing pion energy yielded an angular distribution. This integration was carried out using the trapezoid rule. The cross section was assumed to be negligible at 0 MeV, and, when required, the high-energy end point was extrapolated linearly from the last two measured points. Since in (π^\pm, π^\pm) it was desired to determine the angular distribution for inelastic scattering only, the elastic peak was excluded. Also excluded were the lowest-energy points in the 50° spectra where the cross section appears to rise. It is believed that this increased yield arises from muons which the analysis procedure failed to eliminate. The uncertainty in each differential cross section was calculated as the sum in quadrature of the uncertainty in each trapezoid’s area. The uncertainty in the extrapolation of the end points to zero cross section was estimated to be one-half of the contribution to the integral from the end point regions. In all cases these uncertainties [28] were small compared with the systematic uncertainties discussed in the next section.

The total reaction cross sections were determined by fitting the angular distributions with sums of Legendre polynomials. The regions at forward and backward angles were extrapolated by linearly extending from the extreme measured angles with the slope given by the derivative of the Legendre polynomial sum at that point. Pauli blocking should become important and suppress the cross section for forward angle inelastic scattering. To account for this, forward angle inelastic scattering was extrapolated to 0° at the value of the most forward cross section that was measured. The uncertainty in the total cross section was determined by fitting the Legendre polynomials to the angular distribution plus and minus the uncertainty at each angle. The uncertainty in the extrapolation was determined according to the pre-

³All corrections were applied to these data. In particular, the “cloud muon” correction was different for the spectra from the two targets.

TABLE I. Systematic uncertainties in the experiment.

Reaction	Energy (MeV)	Systematic Uncertainties (%)							
		Angle dependent			Overall normalization				
		Thick. ^a	I.C. ^b	Total	SCATPI	³ He ^c	CH ^d	Total	Overall ^e
³ He(π^- , π^+)	120	4.2	3.0	5.2	2.0	2.0	2.5	3.8	6.4
	180	7.6	2.1	7.9	2.0	2.0	2.5	3.8	8.8
	210	<1.0	3.9	3.9	2.0	2.0	2.5	3.8	5.4
	240	4.5	0.8	4.6	2.0	2.0	10.0	10.4	11.4
³ He(π^- , π^-)	120	4.2	2.4	4.8	2.0	2.0	2.5	3.8	6.2
	180	7.6	1.4	7.7	2.0	2.0	2.5	3.8	8.6
	240	4.5	0.8	4.6	2.0	2.0	10.0	10.4	11.4
³ He(π^+ , π^+)	120	1.9	1.0	2.1	2.0	2.0	2.5	3.8	4.4
	180	3.3	0.5	3.3	2.0	2.0	2.5	3.8	5.1
	240	<1.0	3.2	3.2	2.0	2.0	2.5	3.8	5.0

^aUncertainty in target thickness due to possible misalignment (see text).

^bNormalization uncertainty due to variation in ionization chamber response (see text).

^cUncertainty in ³He target density.

^dUncertainty in CH target density.

^eIncludes angle-dependent and normalization uncertainties only. The uncertainties which depend on the energy of observation are included along with the statistical uncertainties in the plotted error bars.

scription of Kinney [12]. These uncertainties [28] were less than or comparable to the systematic uncertainties discussed in the next section.

H. Systematic uncertainties

There are systematic uncertainties of three types: those that depend on the energy of observation and on the angle of observation, and those associated with the overall normalization. The uncertainty that depends on the energy of observation includes contributions from the electron-pion separation procedure, which typically contributed 2.5%, together with contributions from estimates of the corrections for energy loss and multiple scattering in the target and in the midspectrometer wire chamber, and for effects of pion decay and muon contamination, which contributed an additional 5%. The uncertainty in the correction for energy loss and multiple scattering was estimated to be equal to one-half of the correction applied. The uncertainty in the corrections for pion decay and muon contamination was estimated to be one-half of the difference between the correction derived from the simulation described earlier, and that given by accounting only for the loss of pions by decay within the spectrometer.

An angle-dependent uncertainty (see Table I) arises from possible misalignment between the axis of the target and that of the spectrometer, which will produce changes in both the thickness of the liquid ³He seen by the beam and in the effective acceptance of the spectrometer. These uncertainties were estimated together by comparison between the observed angular variation of the differential cross section for πp scattering and that predicted from interpolation of the known cross sections.

Normalization uncertainties (see Table I) are of two kinds; those that are due to slowly varying changes in the response of the ionization chamber and the density of the ³He target, and those that involve the determination of the absolute scale of the measured cross sections by normalization to πp scattering. Variation in the ionization chamber

response, due to changes in ambient temperature and pressure, was monitored by continuous comparison with the downstream scattering measurement. Since these variations were observed to occur on roughly the same time scale as did changes of spectrometer angle, they were included with the angle-dependent uncertainty. Variation in the target density was estimated by interpolation between recorded observations of the target pressure (temperature). The absolute scale of the cross section involves measurement of the CH target density, which was accurate to 2.5% (except for the thickness used with the 240 MeV negative pion beam, for which the CH target density was known only to 10%), and measurement of the energy of the incident pions which influenced the accuracy of the interpolated cross sections derived from SCATPI [29]. The predictions of the code are accurate to 2%. The uncertainties due to the determination of electronics dead time, spectrometer dispersion, and wire chamber efficiency were insignificant compared to those listed above.

V. RESULTS

A. DCX cross sections

The doubly differential cross sections measured for the ³He(π^- , π^+) reaction at incident energies of 120, 180, and 240 MeV for laboratory angles of 25°, 50°, 80°, 105°, and 130°, and at 210 MeV for 25° and 50° are displayed in Figs. 3–6. A double-peaked structure similar to that observed in ⁴He(π^\pm , π^\mp) [12,13] is clearly seen at forward angles. The double peak disappears with increasing angle, a behavior which was also seen in ⁴He. In the case of ⁴He, the height of the higher-energy peak diminished with decreasing incident pion energy until it completely vanished somewhere between 150 and 120 MeV. In ³He, however, two distinct peaks remain even for energies as low as 120 MeV, although the relative size of the high-energy peak does seem to be diminished. The differential cross sections at each angle are shown in Fig. 7, and the total DCX cross sections for each incident

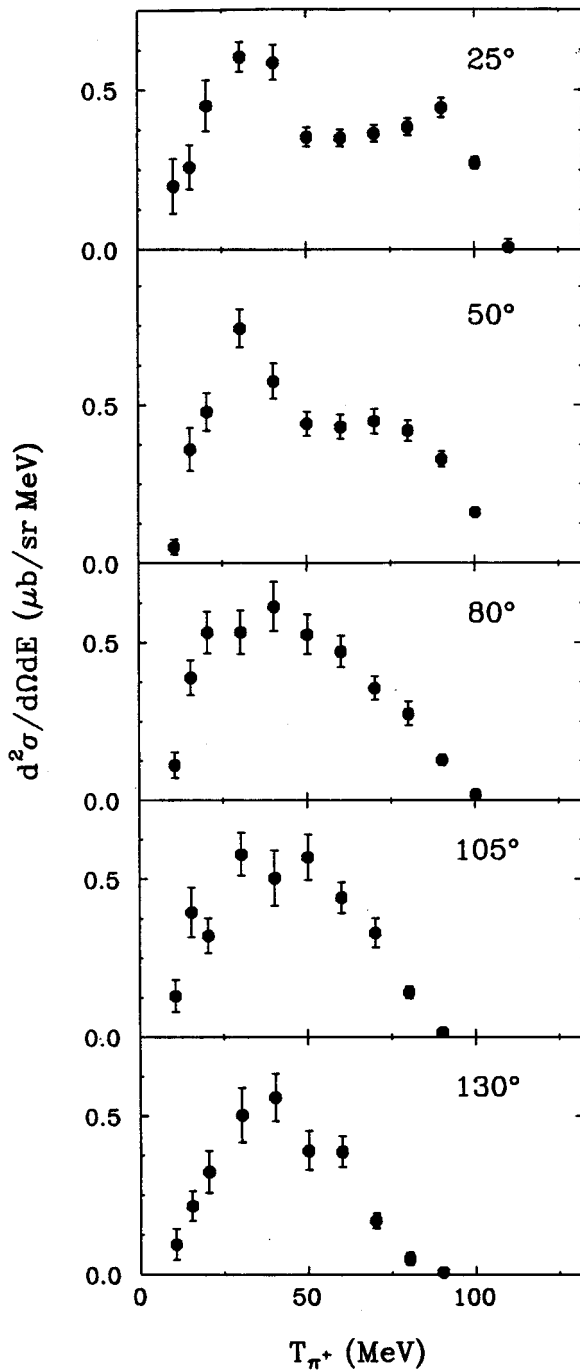


FIG. 3. Doubly differential cross sections for ${}^3\text{He}(\pi^-, \pi^+)$ at 120 MeV for laboratory angles 25° , 50° , 80° , 105° , and 130° . The uncertainties indicated include the statistical uncertainty and the systematic uncertainties which depend on the outgoing pion energy.

energy are listed in Table II. For comparison, Table II also gives the DCX cross sections for ${}^4\text{He}$.

In the present experiment, because only the outgoing π^+ is detected, it was not possible to distinguish between DCX [${}^3\text{He}(\pi^-, \pi^+)3n$] and pion-induced pion production (PIPP) [${}^3\text{He}(\pi^-, \pi^+)\pi^-pnn$]. Pion production is not expected to be a significant source of contamination below about 200 MeV, however, since this reaction can only occur at energies above the threshold at about 170 MeV, resulting

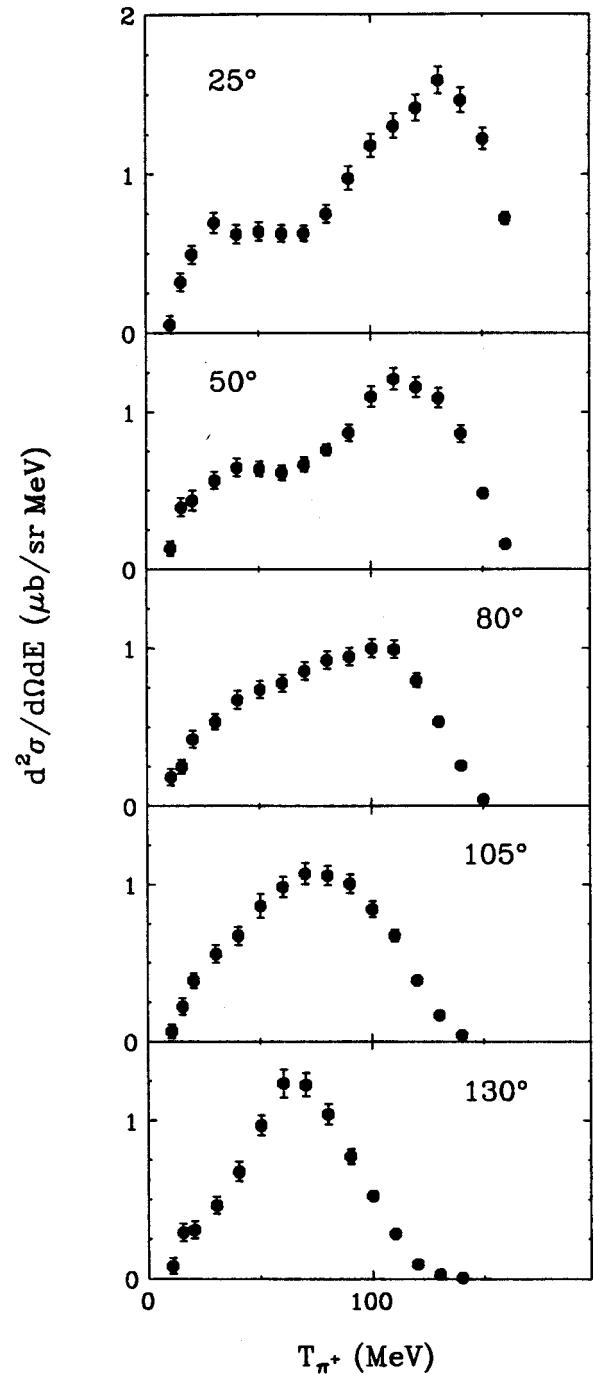


FIG. 4. Same as Fig. 3 but at incident pion energy 180 MeV.

in a severely constrained phase space. Even in the 210 and 240 MeV DCX measurements, the contamination could appear only at the lowest outgoing pion kinetic energies.

To estimate the contribution from PIPP, doubly differential cross sections for the ${}^3\text{He}(\pi^+, \pi^-)$ reaction at 240 MeV were measured (see Fig. 8). With incident π^+ , there is no corresponding DCX reaction. Also plotted in Fig. 8 are the corresponding ${}^3\text{He}(\pi^-, \pi^+)$ doubly differential cross sections for comparison. Integration of the ${}^3\text{He}(\pi^+, \pi^-)$ spectra yields differential cross sections of $5.9 \pm 0.9 \mu\text{b/sr}$ at 25° , and $1.5 \pm 0.4 \mu\text{b/sr}$ at 130° , for 240 MeV incident pions. Since ${}^3\text{He}(\pi^+, \pi^-)$ is at most only about one-tenth of

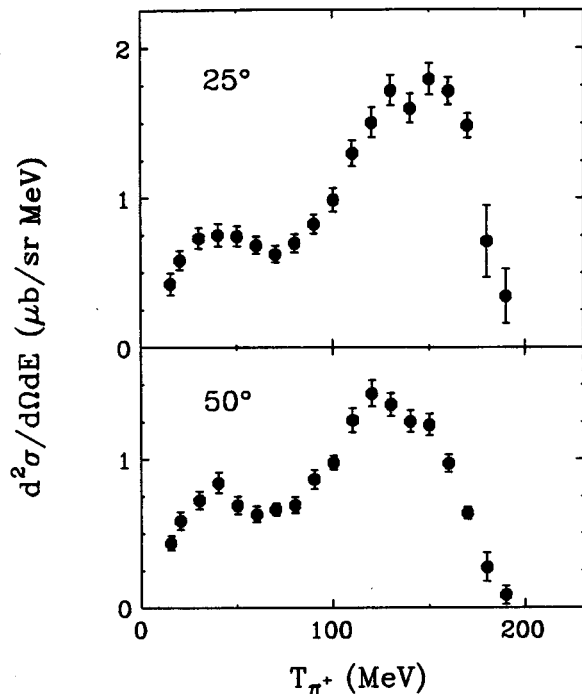


FIG. 5. Same as Fig. 3 but at incident pion energy 210 MeV and laboratory angles 25° and 50° .

the ${}^3\text{He}(\pi^-, \pi^+)$ cross section, one would expect the ${}^3\text{He}(\pi^-, \pi^+)\pi^-pnn$ reaction to make up only about one-fifth of the ${}^3\text{He}(\pi^-, \pi^+)$ cross section. Because pion production is seen to be so much weaker than DCX, and limited to a small range of low outgoing pion energies, no correction for this effect has been made to the DCX cross sections presented.

Doubly differential cross sections for inclusive DCX in intermediate mass nuclei are found to have a shape similar to that predicted by the four-body phase space, corresponding to a pion, two knocked-out nucleons, and the residual nucleus in the final state. Figure 9 compares the present results for ${}^3\text{He}(\pi^-, \pi^+)$ at 180 MeV for laboratory angles of 25° and 130° with the predictions of three-body phase space, i.e., the reaction $\pi^- + {}^3\text{He} \rightarrow \pi^+ + n + (2n)$, where two neutrons recoil together with no internal motion, and with the predictions of four-body phase space, i.e., the reaction $\pi^- + {}^3\text{He} \rightarrow \pi^+ + n + n + n$, where three neutrons recoil independently. As was the case for ${}^4\text{He}$ [12,13], the data do not agree with either phase space prediction.

Figure 10 compares the doubly differential cross sections for ${}^3\text{He}(\pi^-, \pi^+)$ with those for ${}^4\text{He}(\pi^-, \pi^+)$ measured by Kinney *et al.* [12,13]. The most striking difference is the relative size of the two cross sections. In these simple nuclei DCX must result in changing the two available protons to neutrons and one would naively expect the probability of the reactions to be about the same. Apparently, competing processes [31] promoted by the presence of a single additional neutron suppress the DCX cross section in ${}^4\text{He}$. The other major difference between the doubly differential cross sections for ${}^3\text{He}$ and ${}^4\text{He}$ in Fig. 10 is that the spectra for

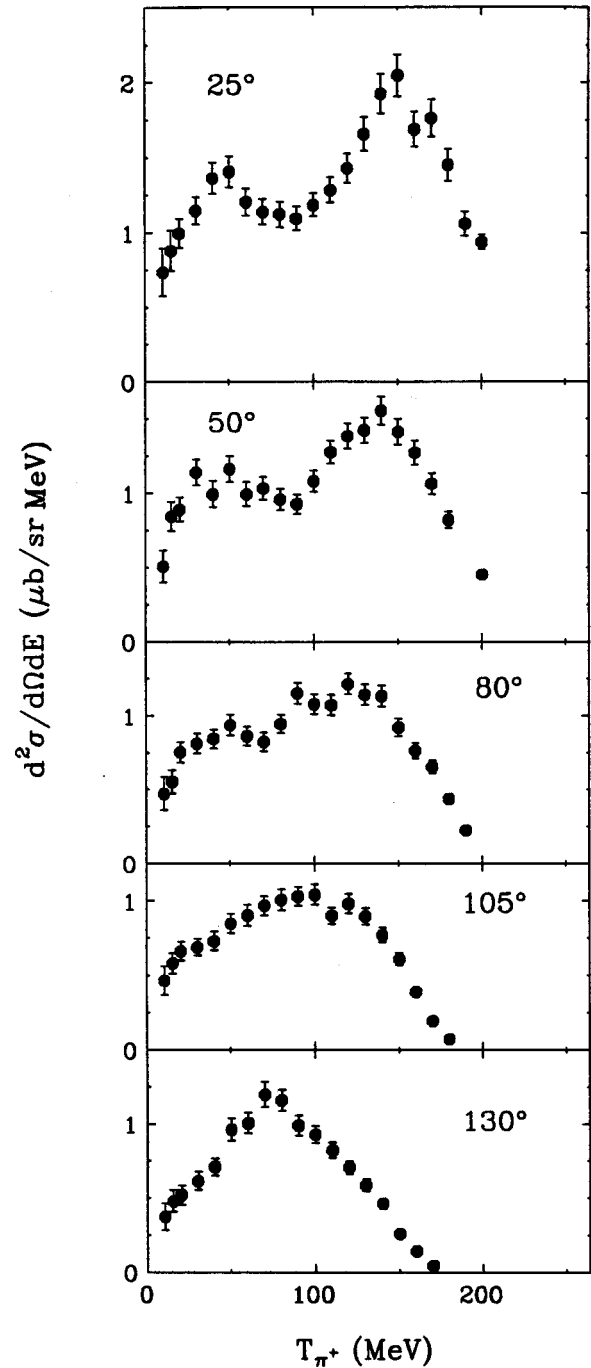


FIG. 6. Same as Fig. 3 but at incident pion energy 240 MeV.

${}^4\text{He}$ appear to be shifted approximately 20 MeV downward⁴ in energy, consistent with the difference between the binding energy of ${}^3\text{He}$ (7.7 MeV) and the binding energy of ${}^4\text{He}$ (28.3 MeV).

The double peaks at forward angles were seen in the earliest DCX experiments on ${}^3\text{He}$ [9]. One early interpretation of the structure was that the higher-energy peak resulted

⁴Although it is difficult to quantify the exact amount the peaks are shifted with respect to each other, the difference in the high-energy end points of the spectra, especially at 130° , is approximately 20 MeV.

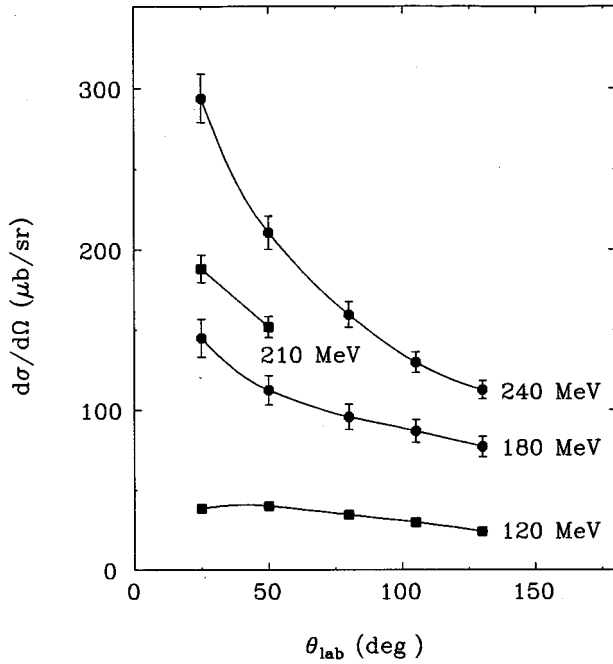


FIG. 7. Angular distributions for ${}^3\text{He}(\pi^-, \pi^+)$ at 120, 180, 210, and 240 MeV. The uncertainties indicated include the statistical uncertainty, the uncertainties arising from the extrapolation and integration procedure (see Sec. IV G), and the systematic uncertainties which depend on the outgoing pion energy and angle.

from the existence of either bound states or broad continuum resonances in the three-neutron system. A three-nucleon resonance with an excitation of 15 MeV had been adduced to explain the continuum neutron spectra in the charge exchange reaction ${}^3\text{He}(p, n)3p$ measured by Williams *et al.* [33], and the first DCX measurements were undertaken, in part, to look for it. Sperinde *et al.* [9] found a double-peaked structure at forward angles similar to that observed in the present experiment, and interpreted it in terms of a three-neutron resonance at an excitation of 12.5 MeV. Later measurements [11] of the ${}^3\text{He}(\pi^-, \pi^+)$ cross section for a wider range of incident energies and observation angles showed similar features, but it was found that they did not imply resonance parameters consistent with those of Sperinde *et al.* or Williams *et al.* Phillips [10] demonstrated that the high outgoing energy peak could be explained by an interaction between two of the neutrons in the final state, and a later theoretical study by Offermann and Glöckle [34] showed that a low-energy resonance in the three-neutron system was

TABLE II. Total cross sections for the ${}^3\text{He}(\pi^-, \pi^+)$ reaction including statistical and all systematic uncertainties. For comparison, ${}^4\text{He}(\pi^+, \pi^-)$ and ${}^4\text{He}(\pi^-, \pi^+)$ total cross sections from Ref. [12] are also listed.

Incident energy (MeV)	Total cross section		
	${}^3\text{He}(\pi^-, \pi^+)$ (μb)	${}^4\text{He}(\pi^+, \pi^-)$ (μb)	${}^4\text{He}(\pi^-, \pi^+)$ (μb)
120	395 ± 28	128 ± 13	—
180	1210 ± 95	489 ± 23	418 ± 25
240	2061 ± 230	1014 ± 37	1075 ± 76

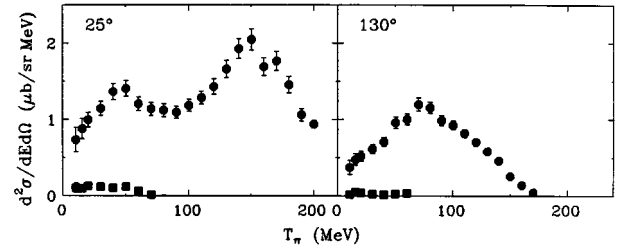


FIG. 8. A comparison of doubly differential cross sections for ${}^3\text{He}(\pi^+, \pi^-)$ (squares) with ${}^3\text{He}(\pi^-, \pi^+)$ (circles) at 240 MeV for laboratory angles 25° and 130° . The uncertainties indicated include the statistical uncertainty and the systematic uncertainties which depend on the outgoing pion energy.

extremely unlikely. For a review of the evidence collected for the existence of 3n bound states and continuum resonances up to 1987, see Ref. [35].

In order to test whether or not the high-energy peak in the present data is caused by a resonance, the four-body phase space distribution for each reaction times a normalization constant was fitted to the lower peak of each DCX spectrum. A Gaussian distribution was fitted to the higher-energy peak, from which the centroid and width of the peak were determined. The missing masses determined for the higher-energy peak varied greatly over the range of energy and angle studied. The excitation energy, which Williams [33] found to be 15 MeV and Sperinde [9] found to be 12.5 MeV, was found in the present work to vary from 19.5 MeV for 25° and 120 MeV to 68.4 MeV for 80° and 240 MeV. The excitation energy seems to increase both with increasing scattering angle and increasing incident energy. Because the variation in the excitation energy is much larger than any possible uncertainty in the measurement, one must conclude that there is no evidence that the high-energy peak is a resonant state of three neutrons in the final state of the reaction ${}^3\text{He}(\pi^-, \pi^+)$.

B. Comparison of DCX results with theoretical calculations

The simplest mechanism that accounts for DCX is sequential single charge exchange (SSCX), as depicted in Fig. 1(a). The double-peaked structure in the DCX spectrum at

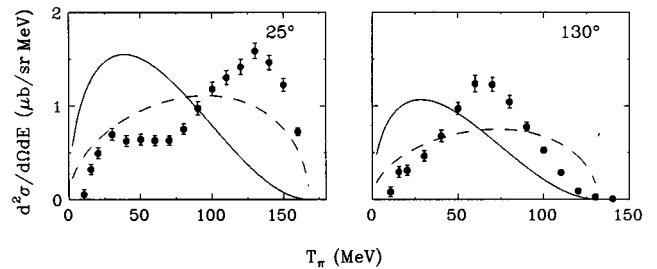


FIG. 9. A comparison of doubly differential cross sections for ${}^3\text{He}(\pi^-, \pi^+)$ with the prediction of three-body (dashed line) and four-body (solid line) phase space at 180 MeV for laboratory angles 25° and 130° . The phase space predictions have been normalized to have the same singly differential cross section as the data. The uncertainty indicated includes the statistical uncertainty and the systematic uncertainties which depend on the outgoing pion energy.

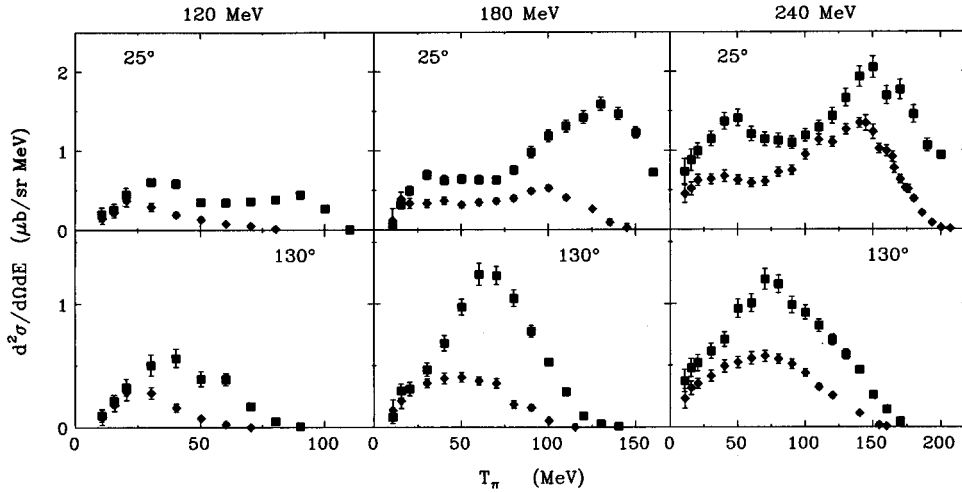


FIG. 10. A comparison of the doubly differential cross sections for ${}^3\text{He}(\pi^-, \pi^+)$ (squares) and ${}^4\text{He}(\pi^-, \pi^+)$ (diamonds) at 180 and 240 MeV for laboratory angles 25° and 130° . Also compared are the cross sections for ${}^3\text{He}(\pi^-, \pi^+)$ (squares) and ${}^4\text{He}(\pi^+, \pi^-)$ (diamonds) at 120 MeV for laboratory angles 25° and 130° . The ${}^4\text{He}$ data are taken from Kinney *et al.* [12,13].

forward angles can be explained as a consequence of the p -wave nature of the single charge exchange (SCX) interaction in the Δ -resonance region, where the SCX cross section is forward and backward peaked. There are three ways in which SSCX can produce DCX at forward angles: successive (a) forward-angle SCX reactions, (b) intermediate-angle SCX reactions, or (c) backward-angle SCX reactions. For forward-angle SCX, the cross section is large while the energy loss is small, so (a) will lead to a high outgoing energy peak. Similarly, (c) will lead to a low outgoing energy peak, since the most energy is lost by pions which scatter backward. In case (b) the cross section for scattering at intermediate angles is relatively small, leading to suppressed DCX cross sections at intermediate outgoing energies. The absence of a double-peaked structure in the spectra from heavy nuclei [14] is presumably the result of initial- or final-state interactions, which will be much more probable in heavy nuclei and will tend to smear out these peaks.

The SSCX model has been the basis of a variety of calculations of DCX [26,36–41]. Almost all have used the fixed scatterer approximation, in which the specific dynamics of the πN interaction are not included, thereby neglecting the propagation of the intermediate Δ within the nucleus as well as ignoring the critical impact of Fermi momenta on the scattering amplitudes. The influence of binding energy is introduced only into the calculation of phase space. Different approximation schemes have been applied, such as classical and semiclassical cascade calculations [26,37,41] and approximate solutions to the Boltzmann equation [40], with varying degrees of success. To date, only the cascade calculations of Oset *et al.* [41,42] attempt to include the effect of the nuclear medium on the intermediate Δ propagation. In the lightest element studied by Oset, ${}^9\text{Be}$, a double-peaked structure is clearly evident, although the shape differs significantly from that measured [42].

Other reaction models besides SSCX have been proposed. One such is the meson exchange mechanism of Germond and Wilkin [43] shown schematically in Fig. 1(b). In their calculation, the DCX reaction proceeds through scattering from exchange mesons in the nucleus. This calculation completely ignored spectator nucleon effects, but nevertheless showed agreement with the energy dependence of the total ${}^4\text{He}$ DCX cross section better than any other early calculation. Later calculations of Robilotta and Wilkin [44] have

shown that when one includes also the contact pion production amplitude with the pion-pion scattering amplitude, the latter mechanism is greatly reduced in strength. The quasi-deuteron absorption mechanism of Jeanneret *et al.* [6], shown in Fig. 1(c), is quite successful in predicting DCX cross sections on ${}^4\text{He}$ at energies above the Δ resonance. In this model, a pion is first produced through the reaction $\pi^+ n \rightarrow \pi^+ \pi^- p$, and then one pion is absorbed on a pn pair. The success of this model at energies above about 280 MeV leads to the conclusion that this three-nucleon process is a major contributor to the DCX cross section above the Δ resonance. Jibuti and Kezerashvili [45] have made predictions using a model which includes SSCX, meson exchange, and more complicated mechanisms. In their calculation, the initial and final (${}^3\text{He}$ and ${}^4\text{He}$) nuclear states were expanded in a hyperspherical basis, and three- and four-body nonlinear differential equations were solved. However, their results are rather difficult to evaluate, as they appear to agree with data [7] which were later shown to be incorrect, as well as with other, presumably correct, data [3].

The semiclassical SSCX calculation for ${}^4\text{He}$ of Kinney [12] took into account several important nuclear medium effects, and predicted doubly differential cross sections that agreed quite well with measured cross sections. We have repeated this calculation for ${}^3\text{He}$. In this model, which is based on formalism developed earlier by Thies and Hüfner [40,46], the incident pion interacts sequentially with the two protons only. Hence only the leading, or “double scattering,” term in the transition matrix is used, i.e.,

$$T = \sum_{i=1}^A \sum_{j \neq i}^A t_i G_0 t_j, \quad (3)$$

where the t_i are the in-medium transition operators for scattering from the i th nucleon, and G_0 is the in-medium pion propagator. The in-medium transition operator is approximated by the free πN transition operator evaluated at an effective relative energy [47]:

$$t_i(E) = t_{\text{free}}(E - T_{\text{c.m.}} - U_i - H_{A-1}), \quad (4)$$

where H_{A-1} is the nuclear Hamiltonian with the dependence on the i th nucleon separated out, $T_{\text{c.m.}}$ is the center-of-mass kinetic energy of the system formed by the i th nucleon and

the incident pion, and U_i is the nuclear potential felt by the i th nucleon. The nuclear potential U_i is approximated by a single constant value U , which is treated as a phenomenological parameter. Using a harmonic oscillator model for ${}^3\text{He}$, the central depth of the potential U was determined from the ${}^3\text{He}$ binding energy to be about 29.4 MeV, while the volume expectation value of the potential is about 17.5 MeV. The transformation of the reaction angle was treated as suggested by Lenz [47]. The free transition matrix element used in the present calculation was derived from the free πN cross section predicted by Arndt [48], which is an empirical energy-dependent phase shift representation of the cross sections.

In order to simplify the calculation, several approximations were necessary. The most severe was neglecting pion absorption. This process is thought to be surface peaked and is assumed to affect the cross section simply as an overall decrease in magnitude, i.e., a reduction of incident flux. Thus, one expects the outgoing pion energy dependence of the calculated doubly differential cross sections to be more accurate than their absolute magnitudes. Effects from coupling to absorption channels in the intermediate or final state are also neglected. However, DCX must involve an isospin $T=1$ nucleon pair, and absorption is not thought to be important in pion interactions with $T=1$ pairs [49]. Plane waves are used to describe the pion and neutron continuum states, neglecting distortions. S -state harmonic oscillator wave functions corrected for nuclear center-of-mass motion were used to describe the protons; the oscillator parameter was determined to be 1.61 fm by reproducing the root-mean-square radius of ${}^3\text{He}$ measured in elastic electron scattering [32,50]. The success achieved by describing quasifree pion scattering as a single nucleon knock-out process [51,23,24] leads to the approximation of treating the intermediate nuclear state as one hole plus one free particle.

Selecting the specific amplitude for scattering from nucleon 1 to nucleon 2, as is shown in Fig. 11, we may write

$$A_{f0}(\vec{k}', \vec{p}_1', \vec{p}_2', \vec{k}) = \int d^3q \int d^3p_2 \langle \vec{k}', \vec{p}_2' | t_2 | \vec{q}, \vec{p}_2 \rangle \langle \vec{p}_2 | \phi_{1s} \rangle \\ \times \frac{1}{E - q^2/2m_\pi - (p_1')^2/2M_N - E_1} \\ \times \int d^3p_1 \langle \vec{q}, \vec{p}_1' | t_1 | \vec{k}, \vec{p}_1 \rangle \langle \vec{p}_1 | \phi_{1s} \rangle, \quad (5)$$

where E_1 is the energy of nucleon 1. This amplitude can be calculated numerically. To simplify the computation, however, the intermediate pion is constrained to propagate classically through the nucleus by performing a Wigner transformation [46] and taking the classical limit $\hbar \rightarrow 0$.

Figure 12 shows the results of this calculation in comparison with the data; the different curves represent different choices for the average nuclear potential. For DCX occurring in the nuclear interior, the mean potential is approximately 29.4 MeV (dot-dashed curves), whereas DCX occurring primarily near the nuclear surface would require a mean potential near zero (dashed curves). The predicted spectra exhibit features qualitatively similar to those seen in the data, namely, a double peak at small angles and a single peak at

larger angles. At incident energy 180 MeV, the calculations generally overestimate the measured cross sections. This is presumably due to the approximation of using plane waves for the pion and knocked-out nucleon wave functions and neglecting pion absorption. At 240 MeV the sensitivity to the potential depth is small, and the calculations provide a good representation of the data for angles forward of 90° .

Given the approximations that have been made in the present SSCX calculation, it is probably not reasonable to expect better agreement with experiment. The fact that the shape and magnitude of the measured cross sections are roughly consistent with the predictions leads to the conclusion that SSCX is the most likely primary mechanism involved in the DCX reaction.

C. Inelastic scattering cross sections

Doubly differential cross sections for the ${}^3\text{He}(\pi^-, \pi^-)$ and ${}^3\text{He}(\pi^+, \pi^+)$ reactions are displayed in Figs. 13–18. These spectra are seen to be dominated by a broad peak near the outgoing pion kinetic energy for free πN scattering. This quasielastic peak is interpreted to be the result of incoherent scattering from each of the nucleons in the target nucleus. In some spectra an elastic scattering peak is also seen at the highest outgoing pion energies. Evidence for multiple scattering is found in the enhanced cross section on the low-energy side of the quasielastic peak in the forward-angle spectra at 180 and 240 MeV. These more complex processes will be discussed later.

It is possible to interpret simply some of the features of the quasielastic peak by a kinematic analysis that includes the Fermi motion of the struck nucleon. The energy loss of the pion can be simply related to the momentum of the nucleons as follows, where the struck nucleon has been assumed to be nonrelativistic:

$$\omega = \frac{q^2}{2M_N} + \frac{\vec{q} \cdot \vec{P}_i}{M_N} + \epsilon, \quad (6)$$

where ω is the energy loss of the pion, \vec{P}_f and \vec{P}_i are the final and incident nucleon momenta, ϵ is the ‘‘separation energy,’’ and $\vec{q} = \vec{P}_f - \vec{P}_i$ is the momentum transfer. This translates to a quasielastic peak centered at $q^2/2M_N + \epsilon$ with

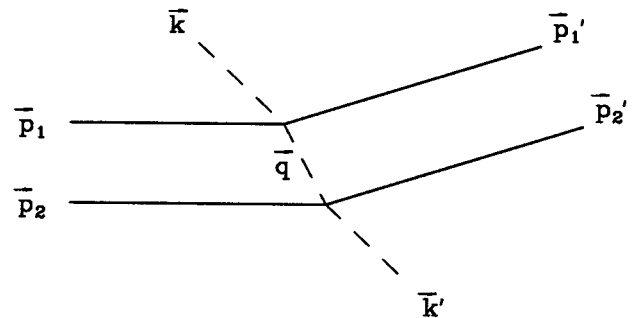


FIG. 11. Diagram of the SSCX process showing the intermediate pion momentum \vec{q} and the incident and knocked-out nucleon momenta \vec{p}_1 , \vec{p}_2 , \vec{p}_1' , and \vec{p}_2' .

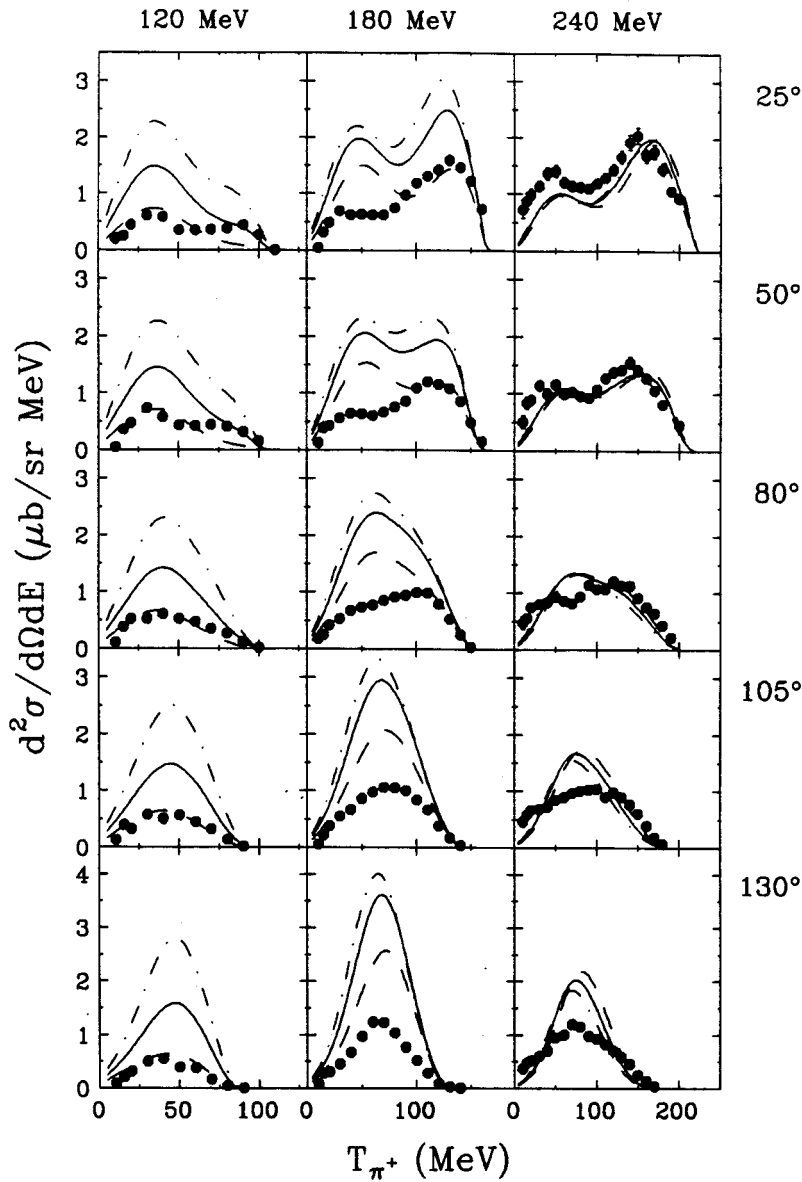


FIG. 12. Doubly differential cross sections resulting from the SSCX calculation of Kinney [12] at 120, 180, and 240 MeV for laboratory angles 25° , 50° , 80° , 105° , and 130° using the average nuclear potentials $U_1=U_2=0$ MeV (dashed line), $U_1=U_2=-17.5$ MeV (solid line), and $U_1=U_2=-29.4$ MeV (dot-dashed line). The points are the result of the present measurement.

a width of $2qP_i/M_N$. The width of the quasielastic peak, σ , and difference between the center of the peak and the average outgoing pion energy for free πN scattering, ϵ , which have been determined by fitting a Gaussian distribution to those doubly differential cross sections greater than one-third of the height of the quasielastic peak, are listed in Table III. The uncertainty in ϵ was estimated to be either the change in ϵ when only cross sections greater than two-thirds of the quasielastic peak were included in the fit, or the change in ϵ required to increase the χ^2 of the original fit by one, whichever was greater.

Moniz [52,53] has shown for electron scattering that a simple Fermi gas model is sufficient to describe the general features of the quasielastic peak, with ϵ being the "average separation energy," and P_i related to the Fermi momentum. For pion scattering, however, a constant "average separation energy" is not sufficient to describe the behavior of ϵ , which varies with incident pion energy. In fact, Δ -hole calculations predict that the value of ϵ should increase with increasing scattering angle [51].

Cross sections for quasielastic scattering from ${}^3\text{He}$ and

${}^4\text{He}$ are compared in Fig. 19. The scale has been adjusted to give both spectra the same maximum to allow easy comparison of the shape. The width of the ${}^3\text{He}$ quasielastic peak, determined by fitting a Gaussian distribution to the data, is 20.2 MeV, which is narrower than the width of the ${}^4\text{He}$ peak (25.7 MeV), and is consistent with the 40% difference seen in electron scattering experiments [54]. Indeed, one expects the ${}^4\text{He}$ peak to be wider, since the nucleons in ${}^4\text{He}$ have a higher Fermi momentum. The ${}^3\text{He}$ quasielastic peak is shifted by 5.2 MeV toward higher energies with respect to the ${}^4\text{He}$ peak, presumably reflecting the difference in separation energy (the binding energy per nucleon in ${}^3\text{He}$ is 2.6 MeV, while in ${}^4\text{He}$ it is 7.1 MeV), plus effects which cause ϵ to vary with incident energy.

Angular distributions for the inelastic scattering processes have been obtained by integrating the spectra of Figs. 13–18 over outgoing pion energy, as described in Sec. IV G. The resulting differential cross sections are shown in Fig. 20. It will be important to keep in mind, in making comparisons with empirical models and theoretical calculations, that these data represent all inelastic, not just quasielastic, processes.

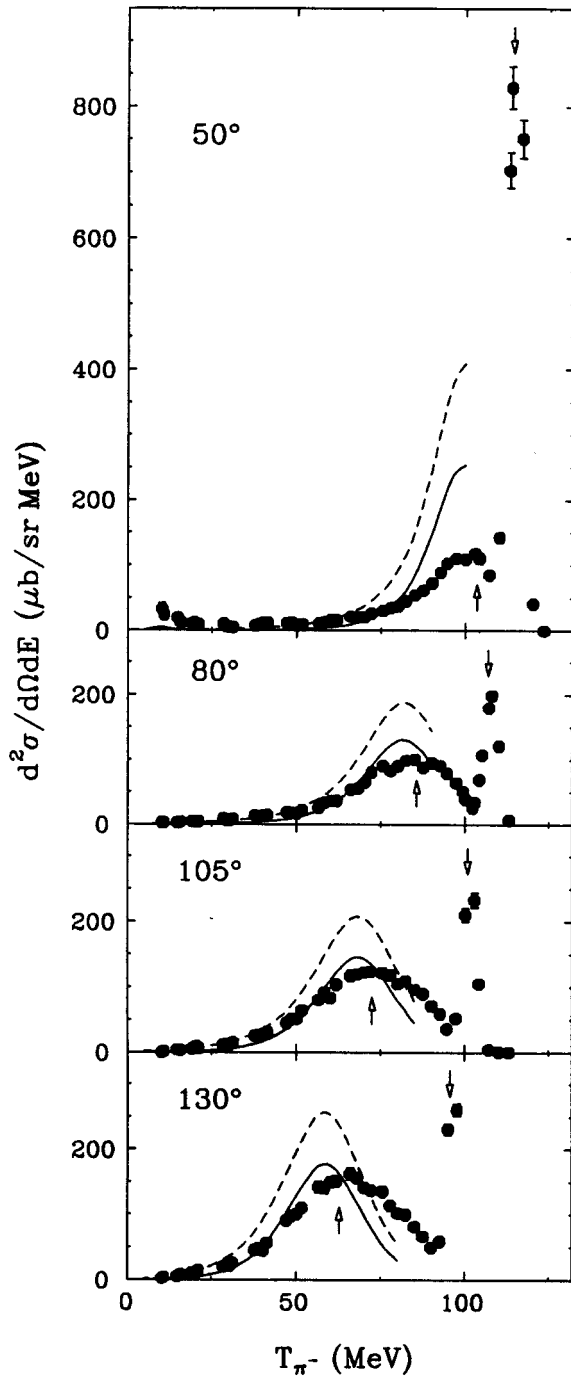


FIG. 13. Doubly differential cross sections for ${}^3\text{He}(\pi^-, \pi^-)$ at 120 MeV for laboratory scattering angles 50° , 80° , 105° , and 130° . The lower-energy arrow indicates the average outgoing pion energy for free πN scattering, while the higher-energy arrow indicates the outgoing pion energy for elastic $\pi-{}^3\text{He}$ scattering. The results of the DWIA calculation using the IEP (dashed line) and FEP (solid line) are also shown. Only the statistical uncertainty and the systematic uncertainties which depend on the outgoing pion energy are indicated.

To compare the differential cross sections for inelastic scattering from ${}^3\text{He}$ with those for scattering from free nucleons, normalized free cross sections were obtained. The normalization factor, \mathcal{N} , is defined via the relation

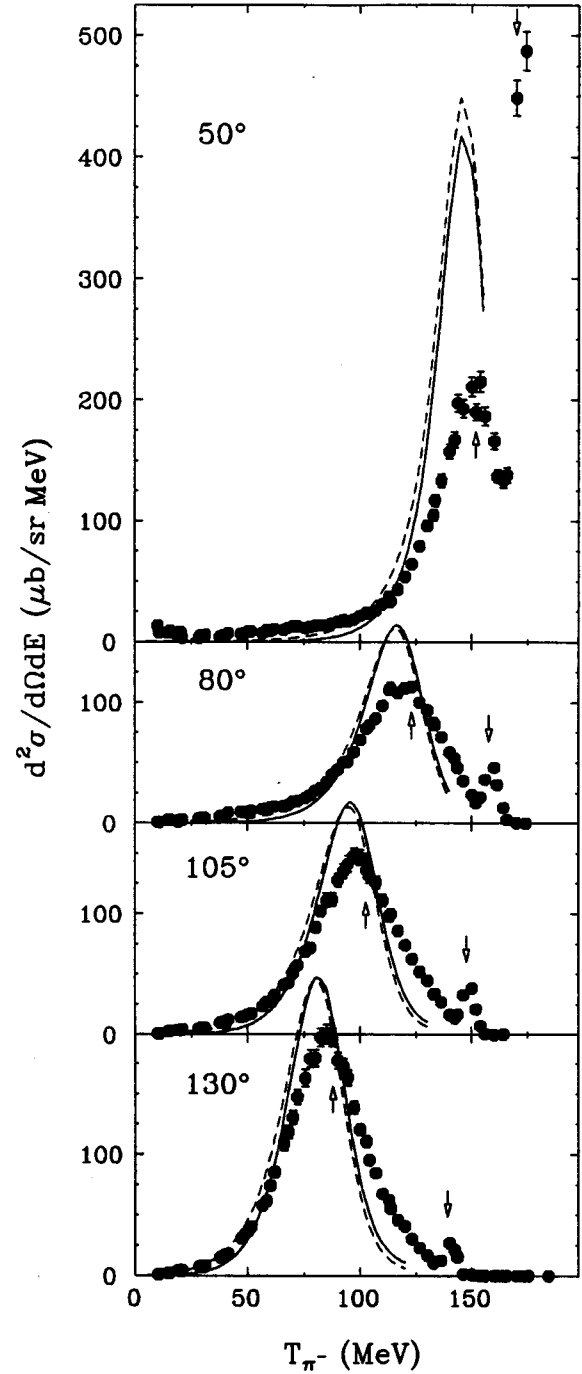


FIG. 14. Same as for Fig. 13 but for 180 MeV incident pions.

$$\frac{d\sigma_{\text{QE}}}{d\Omega} = \frac{\mathcal{N}}{3} \left\{ 2 \frac{d\sigma}{d\Omega}(\pi^{\pm}p \rightarrow \pi^{\pm}p) + \frac{d\sigma}{d\Omega}(\pi^{\pm}n \rightarrow \pi^{\pm}n) \right\}, \quad (7)$$

where the left side represents the cross section for $\pi^{\pm}-{}^3\text{He}$ quasielastic scattering and the differential cross sections on the right side are the free πN cross sections. A value of \mathcal{N} was determined for π^+ and π^- scattering at each incident energy by dividing the measured inelastic scattering cross sections at 105° and 130° (angles where multiple scattering should be negligible) by the average free πN cross

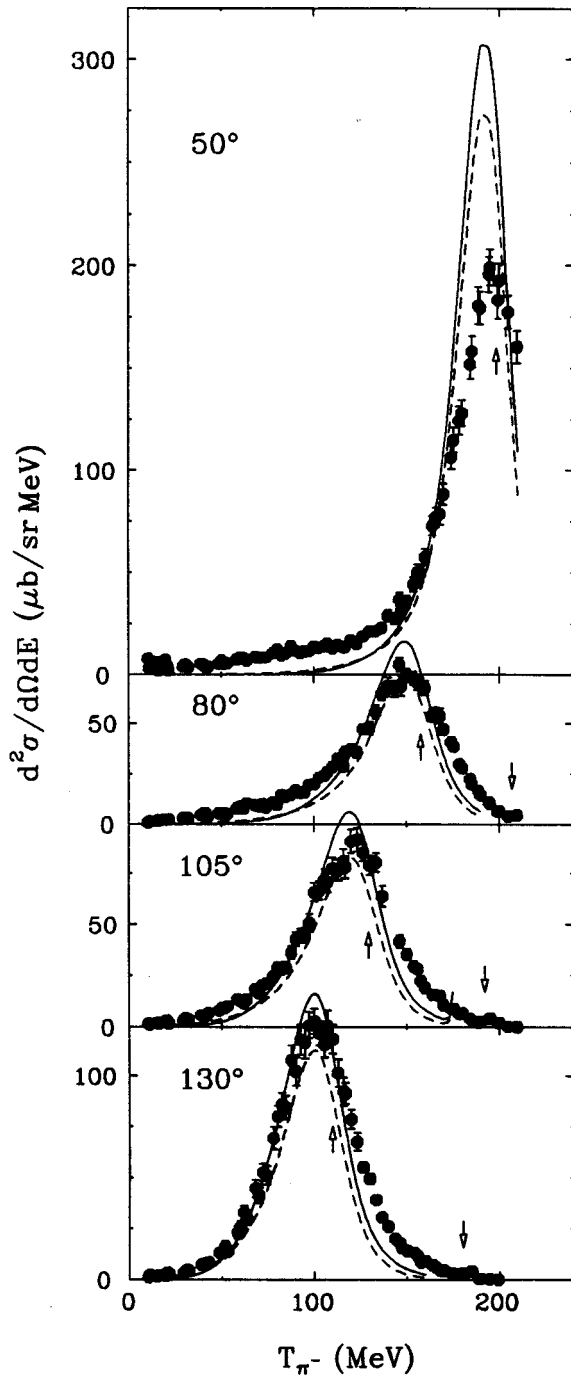


FIG. 15. Same as for Fig. 13 but for 240 MeV incident pions.

sections [see Eq. (7)] given by SCATPI⁵ [29] and taking the weighted means of the results at the two angles. \mathcal{N} was found to vary between 1.6 and 2.6 (see Ref. [28]), with the smallest values occurring at 180 MeV, where the cross section for pion absorption (the dominant effect reducing \mathcal{N} below the “free” value of 3) is the largest.

The dotted curves in Fig. 20 represent the cross sections given by Eq. (7). For π^+ scattering at 180 and 240 MeV, the measured cross sections at 80° lie above the curves, presum-

⁵Charge symmetry was assumed, i.e., $(d\sigma/d\Omega)(\pi^{\pm}n \rightarrow \pi^{\pm}n) = (d\sigma/d\Omega)(\pi^{\mp}p \rightarrow \pi^{\mp}p)$.

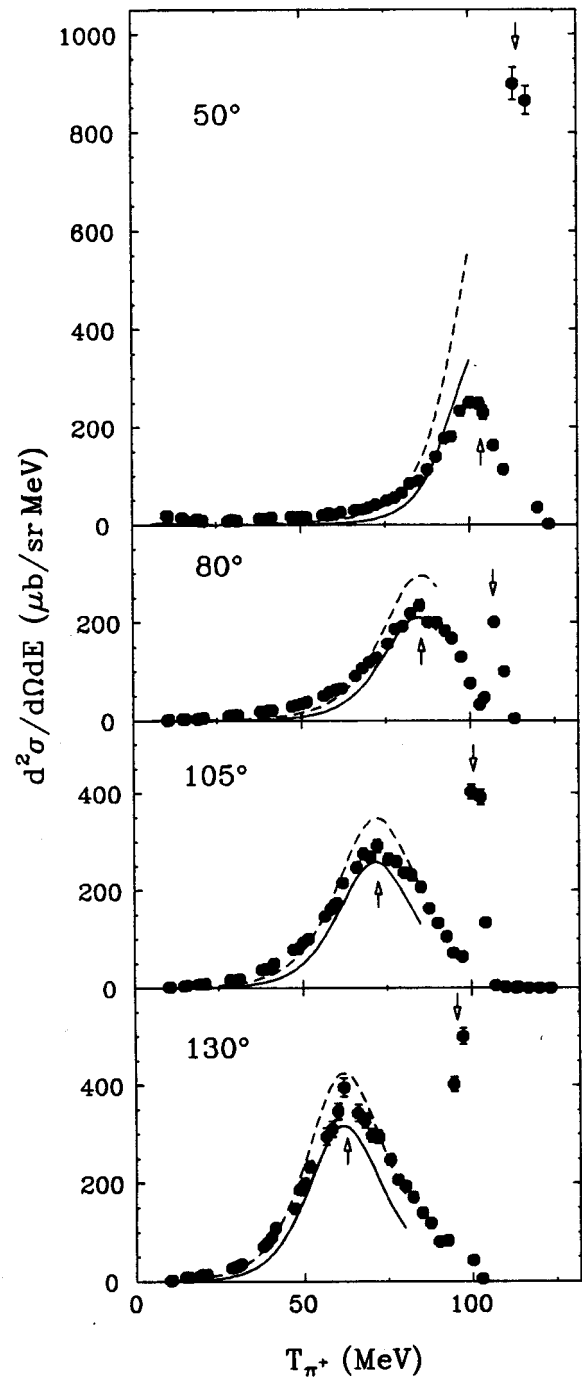


FIG. 16. Same as for Fig. 13 but for ${}^3\text{He}(\pi^+, \pi^+)$.

ably reflecting the presence of multiple scattering. At 50°, the cross sections are below the curves. Although multiple scattering is certainly present (see the prominent “shoulders” on the low-energy sides of the peaks in Figs. 17 and 18), the overall cross section is reduced by Pauli blocking. This latter effect is particularly evident at incident energy 120 MeV, where multiple scattering appears, from the shape of the spectrum, to be small.

D. Comparison of inelastic scattering results with theoretical calculations

The earliest attempt to model inelastic pion scattering used the so-called “pole-mechanism” [55], in which the ma-

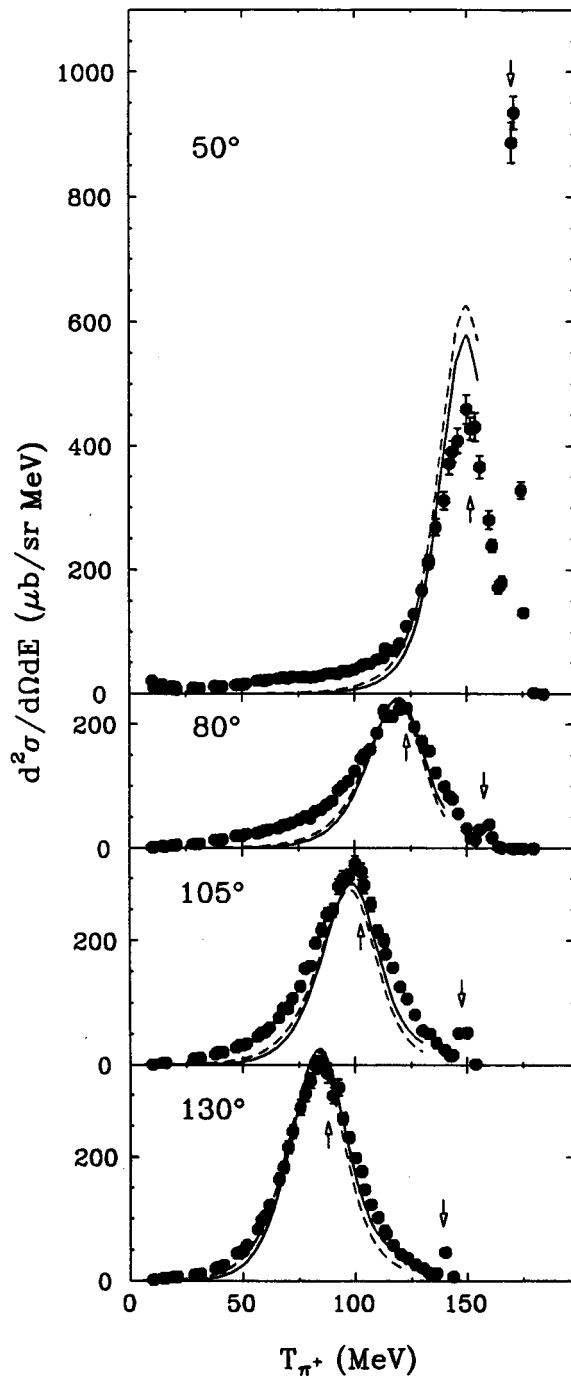


FIG. 17. Same as for Fig. 13 but for ${}^3\text{He}(\pi^+, \pi^+)$ at 180 MeV.

trix element is expressed in terms of a virtual decay $A \rightarrow (A-1) + N$ (determined experimentally from pickup reactions) and free πN scattering. Later, semiclassical models [56,57] were used in which the pions followed straight-line paths through the nucleus, along which they were attenuated. The standard method for describing pion inelastic scattering in the fixed scatterer approximation, however, is the distorted wave impulse approximation (DWIA). In these calculations, the wave function of the incident and final pion, and of any knocked-out nucleons, are distorted by the optical potential of the residual nucleus.

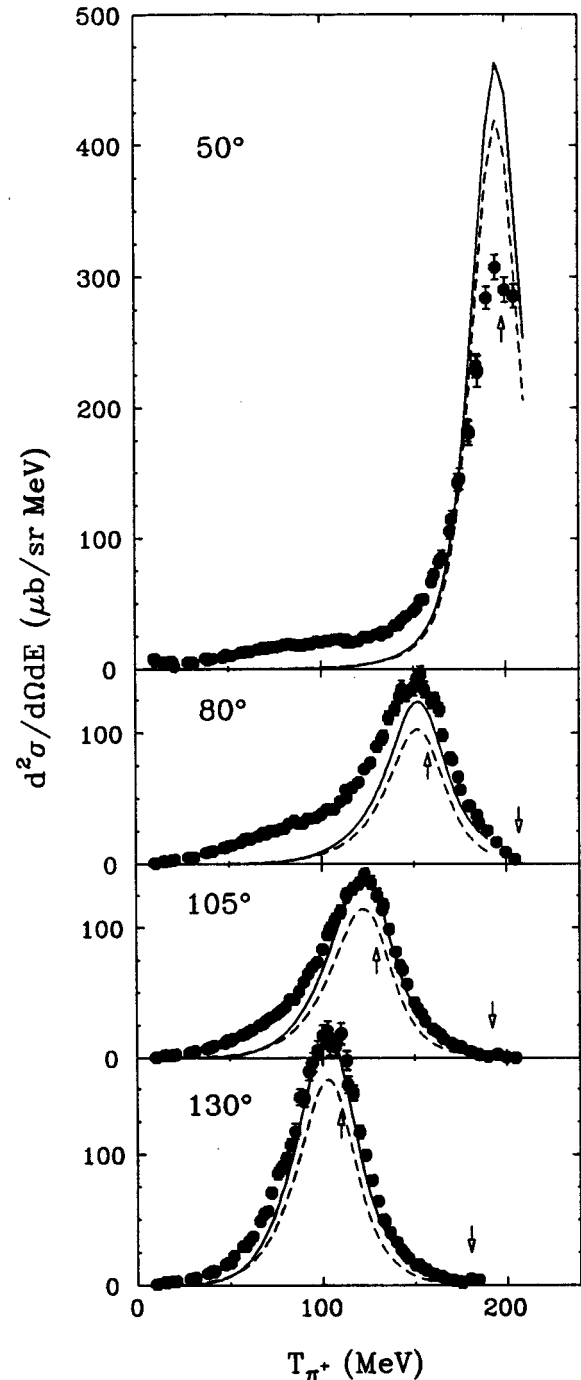


FIG. 18. Same as for Fig. 13 but for ${}^3\text{He}(\pi^+, \pi^+)$ at 240 MeV.

Pion inelastic scattering has also been calculated using the Δ -hole approach, which allows the Δ to propagate through, and interact with, the residual nucleus [47,58–62], but so far there has been no full Δ -hole calculation for inelastic scattering on ${}^3\text{He}$. Calculations for ${}^{16}\text{O}$ [51,63] and ${}^4\text{He}$ [64], however, seem to indicate that Δ propagation and interaction are important effects which must be considered if one is to have a complete picture of the interaction of pions with nuclei.

The general factorized DWIA code THREEDEE of Rees, Chant, and Roos [65,66] has been previously applied to the ${}^3\text{He}$ nucleus by both Klein *et al.* [23] and Khandaker *et al.*

TABLE III. Positions and widths of quasielastic peaks. ϵ is the difference between the average outgoing pion energy for free πN scattering and the energy of the centroid of the quasielastic peak, and σ is the Gaussian width parameter determined by fitting the data as described in the text.

Incident energy (MeV)	Angle	${}^3\text{He}(\pi^+, \pi^+)$		${}^3\text{He}(\pi^-, \pi^-)$	
		ϵ (MeV)	σ (MeV)	ϵ (MeV)	σ (MeV)
120	50°	3.8±0.7	4.2±0.4	3.9±1.0	8.6±1.3
	80°	14.8±2.4	11.2±1.8	12.9±0.4	14.0±1.8
	105°	19.6±1.4	12.2±1.8	18.1±1.4	13.5±3.8
	130°	23.9±0.5	10.4±0.7	24.5±1.1	13.7±2.2
180	50°	3.7±0.4	9.6±1.0	5.2±0.3	12.0±0.8
	80°	9.8±0.9	14.1±0.9	9.7±1.2	15.4±1.1
	105°	14.4±0.5	12.0±1.0	13.8±0.2	15.3±0.2
	130°	19.2±0.2	13.0±0.8	19.2±1.8	14.1±0.5
240	50°	5.4±0.8	14.7±1.7	4.9±0.7	15.2±1.4
	80°	8.4±4.5	18.9±0.3	5.9±3.1	18.2±1.1
	105°	11.1±0.9	18.5±1.6	7.6±1.4	20.8±3.5
	130°	15.0±1.2	15.6±1.0	12.3±0.9	17.3±1.6

[24,25]. These DWIA calculations for ${}^3\text{He}$ were found to agree quite well with the measured shape and magnitude of the quasielastic peak, except at forward angles where the calculations generally overestimated the cross section.

This code has been used to predict the doubly differential cross sections for inelastic scattering from ${}^3\text{He}$ in the kinematics of the present experiment. In this formulation, which assumes a quasielastic mechanism, the knocked-out nucleon (N) and spectator system (S) are explicitly included: ${}^3\text{He}(\pi, \pi'N)S$. The knocked-out nucleon phase space is integrated to produce an inclusive cross section for quasielastic scattering. The cross sections from protons and neutrons are

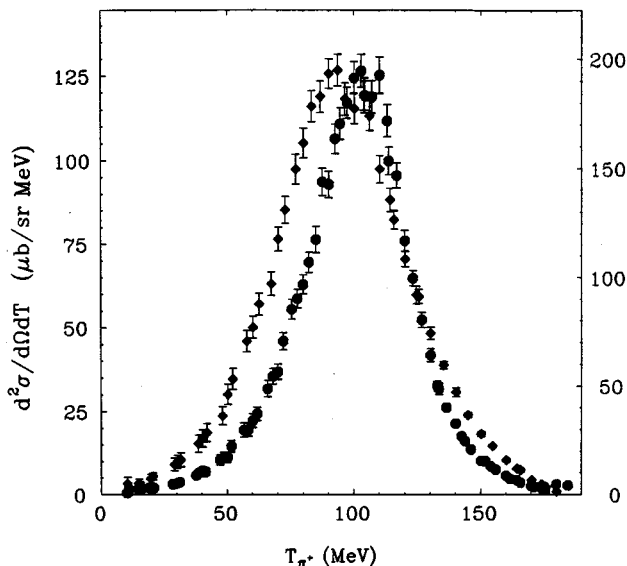


FIG. 19. Comparison of quasifree pion scattering on ${}^3\text{He}$ and ${}^4\text{He}$ at 240 MeV and scattering angle 130° . The circles are the cross sections for ${}^3\text{He}(\pi^+, \pi^+)$ (right-hand scale) from the present experiment, while the diamonds are those for ${}^4\text{He}(\pi^+, \pi^+)$ [12] (left-hand scale).

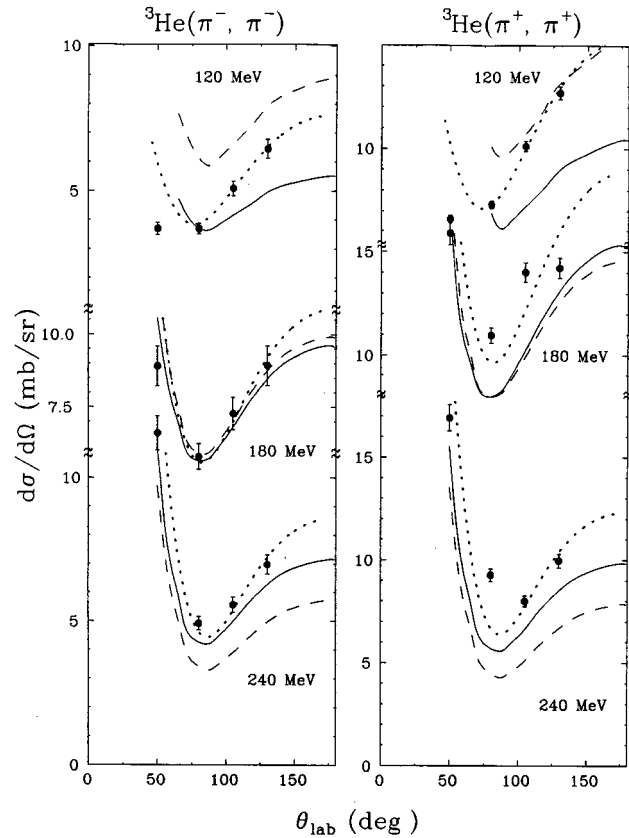


FIG. 20. Angular distributions for ${}^3\text{He}(\pi^-, \pi^-)$ and ${}^3\text{He}(\pi^+, \pi^+)$ compared with the normalized free nucleon cross sections (dotted line, see text) and with the DWIA calculation using the IEP (dashed line) and the FEP (solid line). The uncertainties shown include the statistical uncertainty, the uncertainties arising from the extrapolation and integration procedure, and the systematic uncertainties which depend on the outgoing pion energy and angle.

then weighted by the number of each species present in ${}^3\text{He}$, and summed to form the total quasielastic cross section.

The $(\pi, \pi'N)$ cross section is determined by evaluating the transition matrix for specific initial and final states by factorizing according to the standard DWIA prescription [66], using the single nucleon wave function for ${}^3\text{He}$ of Lim [67]. The incident and final distorted pion wave functions are calculated with a modified Klein-Gordon equation [68] where the potential has the Kisslinger [69] form, using the energy dependence of the s - and p -wave parameters given by Cottingham and Holtkamp [70] and the ${}^3\text{He}$ charge distribution of Ref. [32]. The knocked-out nucleon wave function is distorted according to a Woods-Saxon parametrization of the optical potential in a semirelativistic Schrödinger equation [71], where only the real part of the optical potential is used to describe the inclusive ${}^3\text{He}(\pi, \pi)$ cross section [72]. The half-off-shell transition matrix is approximated by the πN phase shifts of Rowe, Salomon, and Landau [73] according to two simple prescriptions [66]. In the initial energy prescription (IEP), the half-off-shell transition matrix is approximated by the on-shell matrix evaluated at the initial pion energy, while the final energy prescription (FEP) evalu-

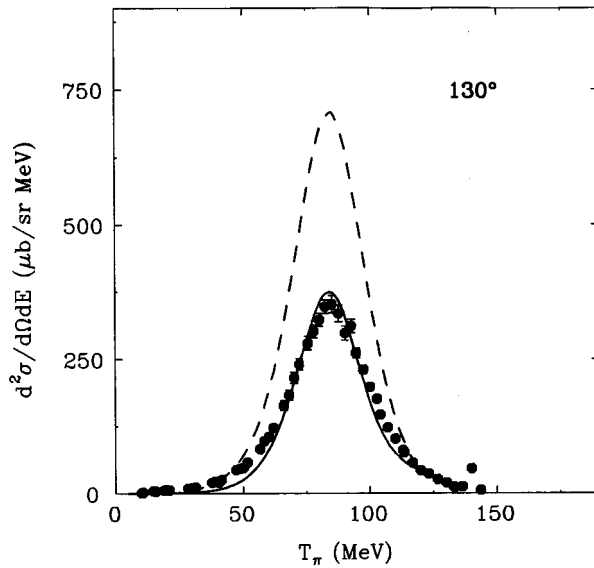


FIG. 21. Comparison of the results of the PWIA (dashed line) and the DWIA (solid line) calculations using the IEP for ${}^3\text{He}(\pi^+, \pi^+)$ at 180 MeV and scattering angle 130° .

ates the on-shell transition matrix at the final (after scattering) pion energy.

The results of the calculation are shown as the dashed (IEP) and solid (FEP) curves in Figs. 13–18. As was found by previous authors [23–25], the calculation reproduces the shapes, positions, and magnitudes of the quasielastic peaks fairly well, except at 50° . Here the calculated cross section is larger than that measured, presumably due to the neglect of Pauli blocking. The positions and widths of the peaks calculated for π^+ scattering are in generally better agreement with the measurement than is the case for π^- scattering, where the calculated peaks (particularly at 120 and 180 MeV) are too narrow and occur at too low an energy. Experimentally the π^\pm peak positions and widths are more nearly similar; if there is any difference it is in the opposite direction: Table III reveals a tendency for a larger width σ and smaller ϵ (thus higher energy) for π^- scattering.

In the energy region below the quasielastic peak the calculation underestimates the measured cross section, particularly at forward angles. This is almost certainly due to multiple scattering with large energy loss, which is not explicitly included. Secondary interactions enter implicitly through the distortions of the outgoing wave by the optical potential, which will redistribute strength from the quasielastic peak to lower outgoing pion energies. The use of an optical potential for ${}^3\text{He}$ is at best naive, especially for the final-state distortions where the pion is in fact interacting with a two-nucleon system following quasifree scattering, and should not be expected to reproduce the measured spectrum in detail. The most important feature of the distorting potential is its large imaginary part arising from pion absorption, which has the effect of reducing the cross section overall by a large factor. This is illustrated in Fig. 21 in which the PWIA result is compared with the DWIA result and with the data for π^+ scattering at incident energy 180 MeV and scattering angle 130° .

TABLE IV. Total inelastic scattering cross sections for the ${}^3\text{He}(\pi^+, \pi^+)$ and ${}^3\text{He}(\pi^-, \pi^-)$ reactions, and predictions of PWIA and DWIA calculations. The uncertainties quoted are discussed in the text.

Incident beam (MeV)	Data	σ_{IS} (mb)			
		PWIA		DWIA	
		(IEP)	(FEP)	(IEP)	(FEP)
120 π^-	60 ± 3	117 ± 14	72 ± 8	91 ± 21	57 ± 13
120 π^+	116 ± 5	177 ± 26	118 ± 18	140 ± 54	95 ± 38
180 π^-	98 ± 8	186 ± 14	177 ± 12	130 ± 8	120 ± 8
180 π^+	169 ± 10	326 ± 28	313 ± 25	160 ± 34	156 ± 29
240 π^-	93 ± 13	114 ± 10	139 ± 10	86 ± 9	108 ± 10
240 π^+	144 ± 11	196 ± 17	234 ± 18	95 ± 15	116 ± 17

The angular distributions predicted by the DWIA calculation are shown in Fig. 20 as the dashed (IEP) and solid (FEP) curves. In comparing the results with the data, it must be remembered that the model assumes a single pion-nucleon interaction, whereas the measurement includes all inelastic scattering processes. The calculated and measured differential cross sections are in better overall agreement for π^- than for π^+ scattering. This agreement may be fortuitous, however, since the calculation did not reproduce the shape and magnitude of the quasielastic peak for π^- scattering. The excess of measured over calculated cross section for π^+ scattering at intermediate angles for 180 and 240 MeV can be traced to the “multiple scattering tail” below the quasielastic peak (see Figs. 17 and 18). At 50° , it appears that the effects of multiple scattering and Pauli blocking conspire to produce a largely fortuitous agreement between experiment and theory. At 120 MeV, the large difference between the calculated results using the IEP and the FEP casts doubt on the validity of either approximation.

In Table IV the predictions of the PWIA and DWIA models for the total inelastic scattering cross sections, σ_{IS} , are compared with the experimental results, obtained by integrating the angular distributions as described in Sec. IV G. The uncertainties in the theoretical cross sections arise from the extrapolation procedures used, which were similar to those used in integrating the experimental data. It is seen that the PWIA grossly overestimates the cross sections, whereas the DWIA predictions are generally consistent with the measurement.

E. Comparison of (π^+, π^+) , (π^-, π^-) , and (π^-, π^+) cross sections

Simple isospin arguments can be used to predict the relative strengths of the inelastic scattering and DCX reactions. For example, using the isospin Clebsch-Gordan coefficients obtained for πN total isospin states, neglecting the $T=1/2$ channel, and assuming quasifree scattering, yields a ratio for π^+ to π^- inelastic scattering cross sections on ${}^3\text{He}$ of 1.73.

Table V shows the ratios of the differential and total cross sections for ${}^3\text{He}(\pi^+, \pi^+)$ to those for ${}^3\text{He}(\pi^-, \pi^-)$. One sees the best agreement with the value of 1.73 at the center of the Δ resonance (180 MeV), as expected. The ratio moves away from 1.73 at higher and lower incident energies. This tendency is also exhibited in the data of Klein *et al.* [23].

TABLE V. Ratios of ${}^3\text{He}(\pi^+, \pi^+)$ to ${}^3\text{He}(\pi^-, \pi^-)$ differential and total cross sections. Statistical and all systematic uncertainties are included.

Incident energy (MeV)	$\sigma(\pi^+)/\sigma(\pi^-)$				
	50°	80°	105°	130°	Total
120	1.78 ± 0.15	1.97 ± 0.15	1.99 ± 0.15	1.96 ± 0.15	1.93 ± 0.14
180	1.78 ± 0.18	1.90 ± 0.19	1.93 ± 0.19	1.59 ± 0.16	1.72 ± 0.18
240	1.46 ± 0.19	1.88 ± 0.23	1.44 ± 0.18	1.43 ± 0.18	1.55 ± 0.24

One can examine the dependence of this ratio on outgoing pion kinetic energy. At the quasielastic peak (especially near the center of the Δ resonance at incident energy 180 MeV), one would expect the ratio to be close to the predicted value of 1.73, since at this energy multiple interactions are presumably relatively unimportant. Figure 22 shows these ratios determined at each angle for 120, 180, and 240 MeV. These ratios are in the general region of 1.73 over most of the range of outgoing pion energy, with close agreement at the quasielastic peak (indicated by arrows). One can calculate the $\sigma(\pi^+)/\sigma(\pi^-)$ ratio assuming only double scattering in the $T=3/2$ channel, with the result 4.48. On the assumption that double scattering becomes increasingly important as the outgoing pion energy decreases, one might expect the measured ratio to rise toward this value with decreasing energy. In general this behavior is not observed, although a rising trend

at 50° and 80° for 180 and 240 MeV can be discerned.

The ratios formed from the doubly differential cross sections at 240 MeV (as in Fig. 22) might be affected by pion-induced pion production (PIPP). Summing the measured single-nucleon PIPP cross sections [74–76] and distributing this total cross section according to four-body phase space to approximate the doubly differential cross section (see Ref. [77]) produces an increase in the ratio of about 5% at an outgoing pion energy of 20 MeV for scattering at 50°.

The reduction of $\sigma(\pi^+)/\sigma(\pi^-)$ may be due to the effect of pion absorption following quasifree scattering. A π^+ will scatter predominantly from a proton, ejecting it from the nucleus, leaving a pn pair, which can absorb the π^+ . A π^- , on the other hand, will scatter predominantly from the neutron, leaving a pp pair. Since absorption on $T=1$ nucleon pairs is strongly suppressed, the π^- has a larger probability of surviving to appear in the spectrum.

The decrease in the ratio seen at very low outgoing pion energies may arise from Coulomb distortions, as the repulsive (attractive) interaction “pushes out” (“pulls in”) the π^+ (π^-) spectra to higher (lower) energy.

Comparison of the PWIA and DWIA calculations described previously can be used to obtain a better understanding of the effects of $T=1/2$ scattering and distortions of the outgoing pion and nucleon waves on the ratio. In the PWIA the ratio remains very nearly 1.73, showing that the $T=1/2$ channel has little effect on the ratio even down to the lowest measured outgoing pion energy. On the other hand, distortion of the outgoing waves, which is included in the ratios calculated in the DWIA, seems to be quite important, causing the ratio to decrease rapidly with decreasing outgoing pion kinetic energy. Some evidence for this behavior is seen in the data, although the calculated effect is generally far too large. This could be due to the choice of pion optical model parameters. To check the validity of the Cottingham-Holtkamp parametrization, the $\pi^\pm - {}^3\text{He}$ elastic scattering cross sections were calculated and compared with data at 120 and 180 MeV (see Ref. [28]). The calculated cross sections are about a factor of 2 too low, suggesting that the absorptive part of the potential is too strong. If absorption were overestimated, $\sigma(\pi^+)/\sigma(\pi^-)$ would be reduced, as discussed above. In a previous study of elastic and inelastic scattering on ${}^3\text{He}$ at 100 MeV, Khandaker [25] found that the potential that best fitted the elastic data had reduced absorption compared with the Cottingham-Holtkamp parametrization, but that the inelastic cross section was relatively insensitive to the choice of optical model parameters.

One can assess the probability of double scattering by comparing the inelastic and DCX data. If much of the

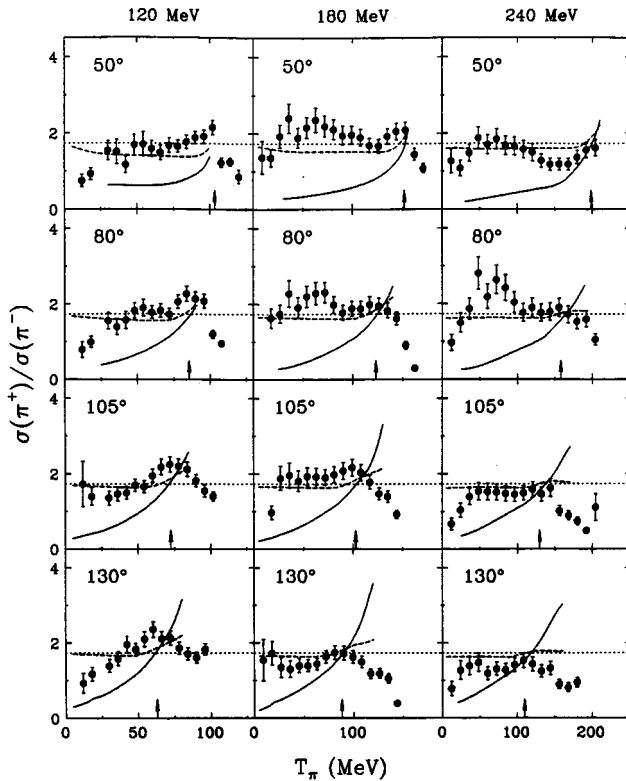


FIG. 22. Ratio of the doubly differential cross sections for ${}^3\text{He}(\pi^+, \pi^+)$ to ${}^3\text{He}(\pi^-, \pi^-)$ determined from the data (points), the PWIA calculation (dashed line), and the DWIA calculation (solid line). The dotted line at 1.73 is the value given by isospin assuming pure $T=3/2$ scattering. The uncertainties indicated include statistical and all systematic uncertainties.

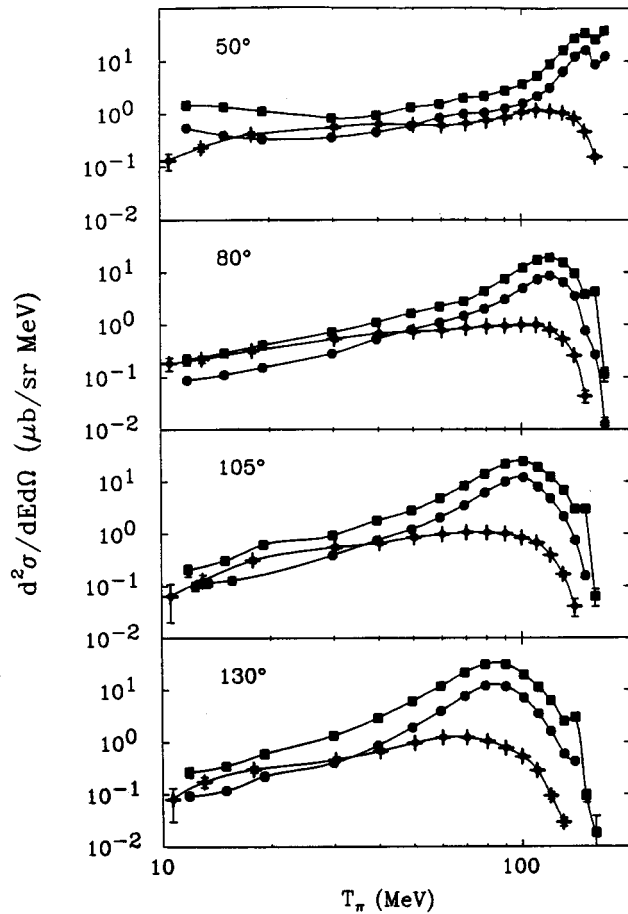


FIG. 23. Comparison of the doubly differential cross sections for ${}^3\text{He}(\pi^+, \pi^+)$ (solid circles), ${}^3\text{He}(\pi^-, \pi^-)$ (solid squares), and ${}^3\text{He}(\pi^-, \pi^+)$ (diamonds) at 50° , 80° , 105° , and 130° for 180 MeV incident pions. The ${}^3\text{He}(\pi^+, \pi^+)$ and ${}^3\text{He}(\pi^-, \pi^-)$ cross sections have been divided by the isospin factors 25.75 and 5.75, respectively (see text).

strength at low outgoing pion energies is due to double scattering, then the low-energy inelastic cross section, scaled to account for isospin, may be similar to the low-energy DCX cross section, which requires interaction with both protons in the ${}^3\text{He}$ nucleus. Figure 23 is a plot of the ${}^3\text{He}(\pi^-, \pi^-)$ and ${}^3\text{He}(\pi^+, \pi^+)$ scattering cross sections compared to the ${}^3\text{He}(\pi^-, \pi^+)$ cross sections at 180 MeV. The ${}^3\text{He}(\pi^-, \pi^-)$ cross sections have been divided by a factor of 5.75 and the ${}^3\text{He}(\pi^+, \pi^+)$ cross sections by 25.75; these factors are obtained from the isospin Clebsch-Gordan coefficients assuming that each reaction proceeds via two steps in the $T=3/2$ channel [78]. One sees that for $T_\pi \leq 50$ MeV the spectra have roughly the same shape and magnitude. The fact that the (π^+, π^+) and (π^-, π^+) cross sections are generally lower than those for (π^-, π^-) can be attributed to absorption competing with the second scattering (or charge exchange) in each of the former cases.

VI. SUMMARY AND CONCLUSIONS

Both DCX and inelastic scattering yield information about the effect of pion multiple scattering in a nuclear tar-

get. To this end, doubly differential cross sections have been measured for the ${}^3\text{He}(\pi^-, \pi^+)$ reaction, and the inelastic ${}^3\text{He}(\pi^+, \pi^+)$ and ${}^3\text{He}(\pi^-, \pi^-)$ reactions at 120, 180, and 240 MeV for scattering angles of 50° , 80° , 105° , and 130° . The DCX cross sections were also measured at 25° , and at 25° and 50° at an incident energy of 210 MeV. Outgoing pions were detected from about 10 MeV up to the kinematic limits. The doubly differential cross sections have been integrated to obtain both angular distributions and total reaction cross sections.

The data have been compared with phenomenological calculations for both the DCX and inelastic scattering reactions. For DCX, a calculation was performed using the semiclassical SSCX model of Kinney [12]. The results of the calculation agree reasonably well with the measured cross sections, considering the nature of the approximations made. The modest success of this calculation in describing the data leads one to believe that SSCX is the dominant mechanism by which the DCX reaction proceeds in this energy range. For inelastic scattering, a DWIA calculation using the method of Chant and Roos [65,66] has been performed. The results of this calculation agree well with the measured cross sections. At low outgoing pion energies, the DWIA calculation underestimates the cross section. This can be understood as a possible effect of multiple scattering, since the DWIA calculation explicitly allowed the pion to interact only once.

The ratio of the ${}^3\text{He}(\pi^+, \pi^+)$ to ${}^3\text{He}(\pi^-, \pi^-)$ cross sections is found to be close to 1.73, the value expected assuming quasifree scattering and $T=3/2$ dominance. The energy dependence of this ratio is better reproduced by the PWIA than by the DWIA calculation, indicating that distortions have been over- (under-) estimated for π^+ (π^-) scattering, or that the measured π^+ cross section has been enhanced by multiple scattering effects, as expected. Additional empirical evidence that multiple scattering is occurring at low outgoing energies is found in the comparison of the inelastic and DCX spectra. Multiple scattering is expected to be an important effect in pion-nucleus reactions because of the strength of the pion-nucleon interaction. In fact, if one assumes that the double scattering component of the inelastic scattering cross section is consistent with the DCX cross section scaled according to isospin considerations, then double scattering seems to account for up to 20–30 % of the inelastic strength.

The DCX and inelastic scattering processes are reasonably well understood phenomenologically. However, a more detailed understanding of the spectra must await more rigorous self-consistent calculations that describe the production and propagation of an intermediate Δ , as well as its interaction with the nuclear medium.

ACKNOWLEDGMENTS

We would like to thank N. Chant and P. Roos for supplying us with their THREEDEE code, and M. Khandaker for his modified version for ${}^3\text{He}$. We would also like to thank R. P. Redwine for many helpful comments. This work was supported in part by funds provided by the U.S. Department of Energy.

- [1] Yu. A. Batusov, S. A. Bunyatov, V. M. Sidorov, and V. A. Yarba, Zh. Éksp. Teor. Fiz. **46**, 817 (1964) [Sov. Phys. JETP **19**, 557 (1964)]; Yad. Fiz. **1**, 383 (1965) [Sov. J. Nucl. Phys. **1**, 271 (1965)]; Yu. A. Batusov, S. A. Bunyatov, V. M. Sidorov, V. A. Yarba, G. Ionice, E. Losnianu, and V. Mihul, *ibid.* **5**, 354 (1967) [**5**, 249 (1967)]; Yu. A. Batusov, S. A. Bunyatov, V. M. Sidorov, and V. A. Yarba, *ibid.* **6**, 998 (1967) [**6**, 727 (1968)]; Yu. A. Batusov, S. A. Bunyatov, N. Dalkhazhav, G. Ionice, E. Losneanu, V. Mihul, V. M. Sidorov, D. Tuvdendorzh, and V. A. Yarba, *ibid.* **9**, 378 (1969) [**9**, 221 (1969)].
- [2] Yu. A. Batusov, S. A. Bunyatov, V. M. Sidorov, and V. A. Yarba, Yad. Fiz. **3**, 309 (1966) [Sov. J. Nucl. Phys. **3**, 223 (1966)].
- [3] L. Gilly, M. Jean, R. Meunier, M. Spighel, J. P. Stroot, P. Duteil, and A. Rode, Phys. Lett. **11**, 244 (1964); L. Gilly, M. Jean, R. Meunier, M. Spighel, J. P. Stroot, and P. Duteil, *ibid.* **19**, 335 (1965).
- [4] N. Carayannopoulos, J. Head, N. Kwak, J. Manweiler, and R. Stump, Phys. Rev. Lett. **20**, 1215 (1968).
- [5] I. V. Falomkin, M. M. Kulyukin, V. I. Lyashenko, G. B. Pontecorvo, Yu. A. Shcherbakov, C. Georgescu, A. Mihul, F. Nichitu, A. Sararu, and G. Piragino, Nuovo Cimento A **22**, 333 (1974).
- [6] J.-B. Jeanneret, M. Bogdanski, and E. Jeannet, Nucl. Phys. **A350**, 345 (1980).
- [7] L. Kaufman, V. Perez-Mendez, and J. Sperinde, Phys. Rev. **175**, 1358 (1968).
- [8] R. E. Mischke, A. Blomberg, P. A. M. Gram, J. Jansen, J. Zichy, J. Bolger, E. Boschitz, C. H. Q. Ingram, and G. Pröbstle, Phys. Rev. Lett. **44**, 1197 (1980).
- [9] J. Sperinde, D. Fredrickson, R. Hinkins, V. Perez-Mendez, and B. Smith, Phys. Lett. **32B**, 185 (1970); J. Sperinde, D. Fredrickson, and V. Perez-Mendez, Nucl. Phys. **B78**, 345 (1974).
- [10] A. C. Phillips, Phys. Lett. **33B**, 260 (1970).
- [11] A. Stetz *et al.*, Nucl. Phys. **A457**, 669 (1986).
- [12] E. R. Kinney, Los Alamos National Laboratory Report No. LA-11417-T, 1988.
- [13] E. R. Kinney, J. L. Matthews, P. A. M. Gram, D. W. MacArthur, E. Piasetzky, G. A. Rebka, Jr., and D. A. Roberts, Phys. Rev. Lett. **57**, 3152 (1986).
- [14] S. A. Wood, J. L. Matthews, E. R. Kinney, P. A. M. Gram, G. A. Rebka, Jr., and D. A. Roberts, Phys. Rev. C **46**, 1903 (1992).
- [15] G. Bernardini, E. T. Booth, L. Lederman, and J. Tinlot, Phys. Rev. **80**, 924 (1950); **82**, 105 (1951); G. Bernardini, E. T. Booth, and L. Lederman, *ibid.* **83**, 1075 (1951).
- [16] M. Camac, D. R. Corson, R. M. Littauer, A. M. Shapiro, A. Silverman, R. R. Wilson, and W. M. Woodward, Phys. Rev. **82**, 745 (1951).
- [17] A. Shapiro, Phys. Rev. **84**, 1063 (1951).
- [18] H. Byfield, J. Kessler, and L. M. Lederman, Phys. Rev. **86**, 17 (1952).
- [19] W. F. Baker, J. Rainwater, and R. E. Williams, Phys. Rev. **112**, 1763 (1958).
- [20] R. M. Edelman, W. F. Baker, and J. Rainwater, Phys. Rev. **122**, 252 (1961).
- [21] F. Binon, P. Duteil, J. P. Garron, J. Gorres, L. Hugon, J. P. Peigneux, C. Schmit, M. Spighel, and J. P. Stroot, Nucl. Phys. **B17**, 168 (1970).
- [22] R. R. Whitney, J. Källne, J. S. McCarthy, R. C. Minehart, R. L. Boudrie, J. F. Davis, J. B. McClelland, and A. Stetz, Nucl. Phys. **A408**, 417 (1983).
- [23] A. Klein, C. Gysin, R. Hennick, J. Jourdan, M. Pickar, G. R. Plattner, I. Sick, and J. P. Egger, Phys. Lett. **B 187**, 253 (1987); Nucl. Phys. **A472**, 605 (1987).
- [24] M. A. Khandaker, M. Doss, I. Halpern, T. Murakami, D. W. Storm, D. R. Tieger, and W. J. Burger, Phys. Rev. C **44**, 24 (1991).
- [25] M. A. Khandaker, Ph.D. thesis, University of Washington, 1987.
- [26] S. A. Wood, Los Alamos National Laboratory Report No. LA-9932-T, 1983.
- [27] C. L. Morris, H. A. Thiessen, and G. W. Hoffmann, IEEE Trans. Nucl. Sci. **NS-25**, 141 (1978).
- [28] M. Yuly, Los Alamos National Laboratory Report No. LA-12559-T, 1993.
- [29] J. B. Walter and G. A. Rebka, Jr., Los Alamos National Laboratory Technical Report No. LA-7731-MS, 1979.
- [30] D. C. Carey, K. L. Brown, and Ch. Iselin, Stanford Linear Accelerator Center Report No. SLAC-246, 1982.
- [31] P. A. M. Gram, S. A. Wood, E. R. Kinney, S. Høibråten, P. Mansky, J. L. Matthews, T. Soos, G. A. Rebka, Jr., and D. A. Roberts, Phys. Rev. Lett. **62**, 1837 (1989).
- [32] J. S. McCarthy, I. Sick, and R. R. Whitney, Phys. Rev. C **15**, 1396 (1977).
- [33] L. E. Williams, C. J. Batty, B. E. Bonner, C. Tschalär, H. C. Benöhr, and A. S. Clough, Phys. Rev. Lett. **23**, 1181 (1969).
- [34] R. Offermann and W. Glöckle, Nucl. Phys. **A318**, 138 (1979).
- [35] D. R. Tilley, H. R. Weller, and H. H. Hasan, Nucl. Phys. **A474**, 1 (1987).
- [36] R. G. Parsons, J. S. Trefil, and S. D. Drell, Phys. Rev. **138**, B847 (1965).
- [37] Yu. A. Batusov, V. I. Kochkin, and V. M. Mal'tsev, Yad. Fiz. **6**, 158 (1967) [Sov. J. Nucl. Phys. **6**, 116 (1968)].
- [38] F. Becker and C. Schmit, Nucl. Phys. **B18**, 607 (1970).
- [39] W. R. Gibbs, B. F. Gibson, A. T. Hess, and G. J. Stephenson, Jr., Phys. Rev. C **15**, 1384 (1977).
- [40] J. Hüfner and M. Thies, Phys. Rev. C **20**, 273 (1979).
- [41] E. Oset, L. L. Salcedo, and D. Strottman, Phys. Lett. **165B**, 13 (1985); L. L. Salcedo, E. Oset, M. J. Vicente-Vacas, and C. García-Recio, Nucl. Phys. **A484**, 557 (1988); M. J. Vicente, E. Oset, L. L. Salcedo, and C. García-Recio, Phys. Rev. C **39**, 209 (1989).
- [42] M. Vicente-Vacas and E. Oset, in *Second LAMPF International Workshop on Pion-Nucleus Double Charge Exchange*, Los Alamos, 1989, edited by W. R. Gibbs and M. J. Leitch (World Scientific, Singapore, 1990), p. 120.
- [43] J.-F. Germond and C. Wilkin, Lett. Nuovo Cimento **13**, 605 (1975); J.-F. Germond and C. Wilkin, in *Mesons in Nuclei*, edited by M. Rho and D. Wilkinson (North-Holland, Amsterdam, 1979), p. 439.
- [44] M. R. Robilotta and C. Wilkin, J. Phys. G **4**, L115 (1978).
- [45] R. I. Jibuti, R. Ya. Kezerashvili, and K. I. Sigua, Phys. Lett. **102B**, 381 (1981); R. I. Dzhibuti and R. Ya. Kezerashvili, Yad. Fiz. **39**, 419 (1984) [Sov. J. Nucl. Phys. **39**, 264 (1984)]; Nucl. Phys. **A437**, 687 (1985); Fiz. Elem. Chastits At. Yadra **16**, 1173 (1985) [Sov. J. Part. Nucl. **16**, 519 (1986)]; Yad. Fiz. **44**, 842 (1986) [Sov. J. Nucl. Phys. **44**, 542 (1987)].
- [46] M. Thies, Ann. Phys. (N.Y.) **123**, 411 (1979).
- [47] F. Lenz, Ann. Phys. (N.Y.) **95**, 348 (1975).
- [48] R. A. Arndt, Z. Li, L. D. Roper, R. L. Workman, and J. M.

- Ford, Phys. Rev. D **43**, 2131 (1991).
- [49] D. Ashery and J. P. Schiffer, Annu. Rev. Nucl. Sci. **36**, 207 (1986).
- [50] R. Mach, F. Nichitu, and Yu. A. Scherbakov, Phys. Lett. **53B**, 133 (1974).
- [51] M. Thies, Nucl. Phys. **A382**, 434 (1982).
- [52] E. J. Moniz, Phys. Rev. **184**, 1154 (1969).
- [53] E. J. Moniz, I. Sick, R. R. Whitney, J. R. Ficenec, R. D. Kephart, and W. P. Trower, Phys. Rev. Lett. **26**, 445 (1971).
- [54] J. S. McCarthy, I. Sick, R. R. Whitney, and M. R. Yearian, Phys. Rev. C **13**, 712 (1976).
- [55] V. M. Kolybasov, Yad. Fiz. **2**, 144 (1965) [Sov. J. Nucl. Phys. **2**, 101 (1966)].
- [56] R. R. Silbar, Phys. Rev. C **11**, 1610 (1975).
- [57] M. M. Sternheim and R. R. Silbar, Phys. Rev. C **21**, 1974 (1980).
- [58] M. Hirata, F. Lenz, and Y. Yazaki, Ann. Phys. (N.Y.) **108**, 116 (1977).
- [59] W. Weise, Nucl. Phys. **A278**, 402 (1977).
- [60] M. Hirata, J. H. Koch, F. Lenz, and E. J. Moniz, Ann. Phys. (N.Y.) **120**, 205 (1979).
- [61] M. Hirata, F. Lenz, and M. Thies, Phys. Rev. C **28**, 785 (1983).
- [62] F. Lenz, M. Thies, and Y. Horikawa, Ann. Phys. (N.Y.) **120**, 266 (1982).
- [63] T. Takaki and M. Thies, Phys. Rev. C **38**, 2230 (1988).
- [64] M. Baumgartner, H. P. Gubler, G. R. Plattner, W. D. Ramsay, H. W. Roser, I. Sick, P. Zupranski, J. P. Egger, and M. Thies, Phys. Lett. **112B**, 35 (1982); Nucl. Phys. **A399**, 451 (1983).
- [65] N. S. Chant and P. G. Roos, Phys. Rev. C **15**, 57 (1977).
- [66] L. Rees, N. S. Chant, and P. G. Roos, Phys. Rev. C **26**, 1580 (1982).
- [67] T. L. Lim, Phys. Lett. **43B**, 349 (1973).
- [68] E. H. Auerbach, D. M. Fleming, and M. M. Sternheim, Phys. Rev. **162**, 1683 (1967).
- [69] L. S. Kisslinger, Phys. Rev. **98**, 761 (1955).
- [70] W. B. Cottingham and D. B. Holtkamp, Phys. Rev. Lett. **45**, 1828 (1980).
- [71] A. Nadasen, P. Schwandt, P. P. Singh, W. W. Jacobs, P. T. Debevec, M. D. Kaitchuck, and J. T. Meek, Phys. Rev. C **23**, 1023 (1981).
- [72] Y. Horikawa, F. Lenz, and N. C. Mukhopadhyay, Phys. Rev. C **22**, 1680 (1980).
- [73] G. Rowe, M. Salomon, and R. H. Landau, Phys. Rev. C **18**, 584 (1978).
- [74] G. Kernel *et al.*, Phys. Lett. B **216**, 244 (1989); **225**, 198 (1989); Z. Phys. C **48**, 201 (1990).
- [75] Yu. A. Batusov, S. A. Bunyatov, G. R. Gulkanyan, V. M. Sidorov, M. Musakanov, G. Ionice, E. Losnianu, V. Mihul, and D. Tuvdendorzh, Yad. Phys. **21**, 308 (1975) [Sov. J. Nucl. Phys. **21**, 162 (1975)].
- [76] J. Lowe *et al.*, Phys. Rev. C **44**, 956 (1991).
- [77] J. Lichtenstadt, D. Ashery, S. A. Wood, E. Piasetzky, P. A. M. Gram, D. W. MacArthur, R. S. Bhalareo, L. C. Liu, G. A. Rebka, Jr., and D. Roberts, Phys. Rev. C **33**, 655 (1986).
- [78] M. L. Dowell, Los Alamos National Laboratory Report No. LA-12691-T, 1994, pp. 122–123.